Published in final edited form as:

Nature. 2022 October ; 610(7933): 768–774. doi:10.1038/s41586-022-05347-z.

HRG-9 homologues regulate haem trafficking from haem-enriched compartments

Fengxiu Sun[1,7], **Zhenzhen Zhao**[1,7], **Mathilda M. Willoughby**[2], **Shuaiqi Shen**[1], **Yu Zhou**[1], **Yiyan Shao**[1], **Jing Kang**[1], **Yongtian Chen**[1], **Mengying Chen**[1], **Xiaojing Yuan**[3,4], **Iqbal Hamza**[3,4], **Amit R. Reddi**[2,5], **Caiyong Chen**[1,6,✉]

[1]MOE Key Laboratory of Biosystems Homeostasis and Protection, College of Life Sciences, Zhejiang University, Hangzhou, Zhejiang, China.

[2]School of Chemistry and Biochemistry, Georgia Institute of Technology, Atlanta, GA, USA.

[3]Department of Pediatrics, Center for Blood Oxygen Transport and Hemostasis, University of Maryland School of Medicine, Baltimore, MD, USA.

[4]Department of Animal and Avian Sciences, University of Maryland, College Park, MD, USA.

[5]Parker H. Petit Institute for Bioengineering and Biosciences and School of Biology, Georgia Institute of Technology, Atlanta, GA, USA.

[6]Cancer Center, Zhejiang University, Hangzhou, Zhejiang, China.

[7]These authors contributed equally: Fengxiu Sun, Zhenzhen Zhao.

Abstract

Haem is an iron-containing tetrapyrrole that is critical for a variety of cellular and physiological processes[1–3]. Haem binding proteins are present in almost all cellular compartments, but the molecular mechanisms that regulate the transport and use of haem within the cell remain poorly understood[2,3]. Here we show that haem-responsive gene 9 (HRG-9) (also known as transport and Golgi organization 2 (TANGO2)) is an evolutionarily conserved haem chaperone with a crucial role in trafficking haem out of haem storage or synthesis sites in eukaryotic cells. Loss of *Caenorhabditis elegans hrg-9* and its paralogue *hrg-10* results in the accumulation of haem

✉**Correspondence and requests for materials** should be addressed to Caiyong Chen. chency@zju.edu.cn.

Author contributions C.C. conceived the project and wrote the manuscript. F.S. and Y.Z. performed the *C. elegans* experiments. F.S., J.K. and Y.Z. conducted the RNA-seq experiment. Z.Z. performed the mammalian cell experiments and haem transfer experiments. M.M.W. and A.R.R. designed and executed the yeast experiments. S.S., Z.Z. and M.C. performed zebrafish experiments. Y.S., F.S. and Y.C. performed haem binding experiments. M.C. performed the immunofluorescence experiments. X.Y. and I.H. contributed to the mammalian haem sensor experiments. All authors discussed the results and commented on the manuscript.

Online content

Any methods, additional references, Nature Research reporting summaries, source data, extended data, supplementary information, acknowledgements, peer review information; details of author contributions and competing interests; and statements of data and code availability are available at https://doi.org/10.1038/s41586-022-05347-z.

Reporting summary

Further information on research design is available in the Nature Research Reporting Summary linked to this article.

Competing interests The authors declare no competing interests.

Supplementary information The online version contains supplementary material available at https://doi.org/10.1038/s41586-022-05347-z.

in lysosome-related organelles, the haem storage site in worms. Similarly, deletion of the *hrg-9* homologue *TANGO2* in yeast and mammalian cells induces haem overload in mitochondria, the site of haem synthesis. We demonstrate that TANGO2 binds haem and transfers it from cellular membranes to apo-haemoproteins. Notably, homozygous *tango2*$^{-/-}$ zebrafish larvae develop pleiotropic symptoms including encephalopathy, cardiac arrhythmia and myopathy, and die during early development. These defects partially resemble the symptoms of human *TANGO2*-related metabolic encephalopathy and arrhythmias, a hereditary disease caused by mutations in *TANGO2*[4–8]. Thus, the identification of HRG-9 as an intracellular haem chaperone provides a biological basis for exploring the aetiology and treatment of *TANGO2*-related disorders.

Haem is an iron-containing cofactor that has essential roles in various biological processes including oxygen transport, electron transport, gene-expression regulation, circadian clock control and signal transduction[1–3]. In humans and most other eukaryotes, haem is synthesized via a conserved, eight-step enzymatic pathway. Although haem is produced in the mitochondrial matrix, haemoproteins and haem-regulated proteins are present in almost all cellular compartments[1]. Given that free haem is hydrophobic and acts as a pro-oxidant, cells must have specific pathways to safely transport haem from mitochondria to extramitochondrial destinations.

C. elegans is an ideal genetic model for studying haem trafficking pathways because it is a haem auxotroph[9]. Previous studies in this model organism have uncovered a number of haem trafficking proteins, including HRG-1, HRG-3, HRG-7 and multidrug resistance protein-5 (MRP-5)[10–13]. In *C. elegans*, haem is assimilated exclusively through intestinal cells from the environment[9]. Besides importing haem from the diet and transferring it to other tissues[10–12], *C. elegans* intestinal cells need to store haem and deliver it to various cellular locations.

hrg-9 is a haem-responsive gene

In an effort to identify new regulators of intestinal haem homeostasis, we performed transcriptomics analysis on intestines isolated from worms that were cultured with low (2 μM), optimal (20 μM) and high (400 μM) concentrations of haem (Extended Data Fig. 1a). Gene-expression profiling revealed a total of 578 genes, including five previously reported haem-responsive genes, that were differentially expressed between these conditions (Fig. 1a and Supplementary Table 1). We found a previously uncharacterized gene, *R186.1*, that was upregulated more than 30-fold by low haem (Fig. 1a,b). Quantitative reverse-transcription PCR (RT–qPCR) analysis confirmed that *R186.1* was regulated by haem (Fig. 1c). *R186.1* has a putative paralogue in *C. elegans*, *Y80D3A.9*, and both genes encode soluble proteins with unknown function. Following the guidelines for nematode genetic nomenclature, we termed *R186.1* and *Y80D3A.9* as *hrg-9* and *hrg-10*.

Transgenic analysis revealed that the *hrg-9* transcriptional reporter (*hrg-9p::gfp*) was expressed predominantly in the worm intestine throughout all developmental stages (Fig. 1d and Extended Data Fig. 1b). Consistent with the results of the RNA sequencing (RNA-seq) analysis, the intestinal expression of *hrg-9p::gfp* was strongly induced under low haem conditions (Fig. 1e). We also generated a transgenic worm line carrying *hrg-10p::gfp*, which

displayed strong expression in the intestine and weak expression in the hypodermis (Fig. 1f and Extended Data Fig. 1c). Together, these results demonstrate that *hrg-9* is a haem-responsive gene specifically induced by haem deficiency in the worm intestine.

Loss of *hrg-9* impairs haem homeostasis

HRG-9 and HRG-10 showed homology with proteins of the TANGO2 family, which was originally identified as a regulator of protein transport and Golgi organization by a functional RNAi screen[14]. To test whether HRG-9 and HRG-10 have a role in protein secretion, we silenced both genes in the VIT-2::GFP transgenic worm, which secretes YP170–GFP from the intestine and delivers it to maturing oocytes[15]. Deficiency of *hrg-9* and *hrg-10* did not impair the secretion of YP170–GFP (Extended Data Fig. 1d), suggesting that these two genes are not required for protein secretion. Moreover, the translational fusion proteins HRG-9::GFP and HRG-10::GFP localized to the cytoplasm, nucleus and apical membrane, but not to Golgi (Fig. 1g).

Given that the expression of *hrg-9* is regulated by haem, we examined whether it regulates haem homeostasis using the IQ6011 haem sensor (*hrg-1p::gfp*)[10]. *hrg-1* is a haem-responsive gene encoding a lysosome-related organelle (LRO) haem transporter in *C. elegans*[10]. Knockdown of *hrg-9* resulted in a haem deficiency response, as indicated by enhanced GFP signals in the IQ6011 worms (Fig. 1h,i). A haem deficiency response was also observed in worms with *hrg-10* RNA-mediated interference (RNAi) (Fig. 1h,i), although its expression was not regulated by haem levels (Extended Data Fig. 1e–g). To corroborate these data, we generated *hrg-9*(*cck301*) and *hrg-10*(*cck302*)-knockout worms and crossed the mutants with the haem sensor strain (Extended Data Fig. 2a). Consistent with the results from RNAi, the expression of *hrg-1p::gfp* as well as that of endogenous *hrg-1* was increased in worms deleted for *hrg-9*, *hrg-10* or both (Fig. 1j–l).

To verify that HRG-9 and HRG-10 regulate haem homeostasis, we fed the worms with gallium protoporphyrin IX (GaPP), a toxic haem analogue that is known to be transported by the haem trafficking pathway[9,10,12]. In the presence of 0.5 μM GaPP, wild-type worms were severely growth arrested, whereas the majority of *hrg-9* and *hrg-10* mutant worms were able to grow to adulthood (Fig. 1m). Additionally, most of the mutant worms survived 1 μM GaPP, a dose that is lethal to wild-type worms (Fig. 1n). Collectively, these data suggest that knockout of *hrg9* and *hrg-10* caused either reduced haem uptake or enhanced haem sequestration in the worm intestine.

HRG-9 is required for LRO haem export

Quantification of haem revealed that the organismal haem content was not reduced in *hrg-9* and *hrg-10* knockout worms (Fig. 2a). Additionally, the uptake of a stable isotope-labelled haem, ^{15}N-haem, by the mutants was similar to that by wild-type worms (Fig. 2b and Extended Data Fig. 2b,c). Thus, the haem deficiency response observed in the mutants was not attributed to reduced haem assimilation.

We next investigated the intracellular haem distribution using a fluorescent haem analogue, zinc mesoporphyrin IX (ZnMP). Compared with wild-type worms, *hrg-9*- and *hrg-10*-

knockout worms exhibited increased ZnMP staining in the intestine, which was further enhanced in the double-knockout worm (Fig. 2c,d). Consistently, knockdown of *hrg-9* or *hrg-10* by RNAi also resulted in ZnMP accumulation (Extended Data Fig. 2d,e). This phenotype was caused specifically by deficiency of *hrg-9* and *hrg-10*, as it could be rescued by the expression of HRG-9::GFP and HRG-10::GFP (Extended Data Fig. 2f). Within worm intestinal cells, ZnMP predominantly colocalized with LysoSensor Green and PGP-2::GFP, markers of LROs[16,17] (Extended Data Fig. 2g,h). Silencing of *pgp-2*, a gene required for LRO biogenesis[16], resulted in significantly reduced ZnMP fluorescence in both wild-type and mutant worms (Fig. 2e,f). These results suggest that loss of *hrg-9* and *hrg-10* leads to haem accumulation in LROs, which have been demonstrated to be the haem storage site in worms[18].

While ZnMP pulse–chase assays revealed no difference in the initial rates of ZnMP accumulation (Fig. 2g), clearance of ZnMP was significantly delayed in worms deficient in *hrg-9* and *hrg-10* (Fig. 2h), suggesting that HRG-9 and HRG-10 control haem efflux out of LROs. This role resembles that of the known LRO haem transporter HRG-1[10]. Silencing of *hrg-1* further exacerbated ZnMP accumulation in *hrg-9* and *hrg-10* mutant worms (Fig. 2i,j), suggesting that HRG-9 and HRG-10 regulate LRO haem export through a HRG-1-independent pathway.

Yeast Tango2p regulates haem homeostasis

The budding yeast *Saccharomyces cerevisiae* expresses an uncharacterized protein, Ygr127wp, that shares approximately 26% identity with *C. elegans* HRG-9 and human TANGO2. Deletion of yeast *tango2* caused a severe growth delay, and this defect could not be complemented by the haem synthesis intermediate 5-aminolevulinic acid (Extended Data Fig. 3a). The total haem level in *tango2Δ* cells was slightly lower than that in the wild-type yeast (Fig. 3a). Using a genetically encoded fluorescent haem sensor targeted to cytoplasm[19], we found that deletion of *tango2* resulted in a modest but significant reduction in cytosolic haem, as demonstrated by the increased ratio of EGFP to mKATE2 fluorescence (Fig. 3b). By contrast, fluorescence assays on the mitochondrial haem sensor revealed a marked increase in the steady-state labile haem level in the mitochondria of *tango2Δ* yeast (Fig. 3c). This accumulation was probably owing to defective mitochondrial haem export, as it could be blocked by succinylacetone, a potent haem synthesis inhibitor[20] (Fig. 3c). The perturbed haem homeostasis was validated further by the abnormal activity of the haem-regulated transcription factor Hap1. The expression of the Hap1 target genes *CYC1* and *CTT1* was enhanced in *tango2Δ* yeast (Fig. 3d and Extended Data Fig. 3b). Since yeast Hap1 localizes to both the nucleus and mitochondria[21], the enhanced activity of Hap1 may be due to the increased haem in mitochondria.

To further characterize the haem defects caused by *tango2* deficiency, we monitored the haem distribution kinetics[22]. Whereas the overall dynamics of labile haem bound to mitochondrial and cytosolic haem sensors were similar between wild-type and *tango2Δ* yeast, the rate of haem trafficking to the nucleus was severely reduced in *tango2Δ* cells (Fig. 3e and Extended Data Fig. 3c,d). Together, these results suggest that the yeast homologue of HRG-9 has an essential role in controlling cellular haem distribution.

TANGO2-knockout mammalian cells

Mutations in human *TANGO2* are known to cause a hereditary disease characterized by encephalopathy, arrhythmias, rhabdomyolysis and metabolic crisis[4–8]. Human TANGO2 localized mainly to the cytoplasm and mitochondria (Extended Data Fig. 3e), a pattern that is consistent with a previous report[7]. However, TANGO2 was not detected in purified mitochondria, implying that it may associate only loosely with mitochondria (Extended Data Fig. 3f)).

Knockout of *TANGO2* in human embryonic kidney (HEK293) cells led to a modest but significant increase of the haem content (Fig. 3f and Extended Data Fig. 3g,h). Inhibition of haem synthesis with succinylacetone eliminated this difference (Extended Data Fig. 3i), indicating increased haem synthesis in *TANGO2*-deficient cells. By fractionating cells into mitochondrial and non-mitochondrial fractions, we found that the mitochondrial haem was significantly increased in *TANGO2*-knockout cells (Fig. 3g,h). To verify this result, we used the haem reporters cyto-APX and mito-APX, which sense labile haem levels in the cytosol and mitochondria, respectively[23]. Consistently, knockout of *TANGO2* caused a significant increase in the mitochondrial labile haem, whereas no difference was detected in the cytosolic labile haem (Fig. 3i).

To ascertain the role of mammalian TANGO2 in haem homeostasis, we deleted *Tango2* in the mouse Friend erythroleukaemia (MEL) cell line (Extended Data Fig. 3j,k), a model cell line commonly used to study haem metabolism. Loss of *Tango2* resulted in reduced haem production and haemoglobinization in MEL cells (Fig. 3j and Extended Data Fig. 3l). Moreover, the *Tango2*-deficient MEL cells exhibited decreased haem in the cytosolic fraction but increased haem in mitochondria (Fig. 3k,l). Thus, TANGO2 may facilitate haem trafficking out of mitochondria.

Since mitochondrial haem overload has been reported to negatively regulate mitochondrial coupling[24], we analysed the effect of *TANGO2* deficiency on mitochondrial respiration. Deletion of *TANGO2* increased the oxygen consumption rates in both HEK293 and MEL cells (Fig. 4a,b and Extended Data Fig. 3m,n). By contrast, the mitochondrial membrane potential and amount of ATP were both reduced in *TANGO2*-deficient cells (Fig. 4c,d and Extended Data Fig. 3o). These observations suggest that the loss of *TANGO2* diminished the coupling of mitochondrial respiration to ATP production, a defect that was probably caused by increased mitochondrial haem.

Loss of *tango2* is lethal to zebrafish

To determine the physiological function of TANGO2 in vertebrates, we generated a *tango2*-knockout (*tango2*$^{-/-}$) zebrafish model (Extended Data Fig. 4a). This mutant contains a 20-bp deletion at the second exon–intron boundary, resulting in intron 2 retention and premature termination (Extended Data Fig. 4b–d). The homozygous *tango2* mutants produced by heterozygous parents were able to grow to adulthood without notable symptoms. However, their progeny all died between 5 and 15 days after fertilization (Fig. 4e). This phenomenon, as well as the presence of maternal *tango2* mRNA in fertilized zebrafish eggs (Extended

Data Fig. 4e), indicates a maternal effect of *tango2*. The loss of *tango2* did not induce obvious defects in haem synthesis and erythropoiesis in early embryos (Extended Data Fig. 4f–i). However, the *tango2*$^{-/-}$ larvae developed symptoms including body rollover, pericardial oedema, deflated swim bladder and reduced locomotor activity at around 2 days before death (Fig. 4f,g and Extended Data Fig. 4j,k).

The deletion of *tango2* in zebrafish also led to defects in the brain, heart and skeletal muscle. Brain micro-computed tomography (micro-CT) scans revealed widening of longitudinal fissures in morbid *tango2*$^{-/-}$ larvae (Fig. 4h and Extended Data Fig. 5a), which is indicative of brain atrophy. The morbid larvae also showed increased expression of *c-fos*, a marker commonly used for neuronal activity (Extended Data Fig. 5b). In addition, the morbid *tango2*$^{-/-}$ larvae exhibited cardiac arrhythmias and slower heart rates with prolonged diastolic filling time (Fig. 4i and Extended Data Fig. 5c–e). Histological analysis revealed disrupted morphology and integrity of muscle fibres in *tango2*$^{-/-}$ larvae (Fig. 4j). This phenotype was further verified by the birefringence assay and actin staining with phalloidin (Fig. 4k,l). These combined defects partially resemble encephalopathy, cardiac arrhythmias and rhabdomyolysis, which are the major symptoms of the *TANGO2* disease.

TANGO2 transfers haem in vitro

When ectopically expressed in the *hrg-9* and *hrg-10*-knockout worm, *TANGO2* genes from yeast, zebrafish and humans were all able to rescue the LRO haem accumulation phenotype (Extended Data Fig. 6a), suggesting that HRG-9 and TANGO2 have a conserved role in exporting haem out of membrane-enclosed organelles. To substantiate this role, we performed haem transfer assays using mitochondria isolated from HEK293 cells as the haem donor and apo-myoglobin as the haem acceptor. Addition of the recombinant human TANGO2 protein markedly enhanced the haem activity in myoglobin (Fig. 5a). Similarly, human, yeast and zebrafish TANGO2 proteins all stimulated the transfer of haem from mitochondria isolated from mouse livers to apo-myoglobin (Fig. 5b and Extended Data Fig. 6b,c), whereas BSA and GFP had no such activity (Extended Data Fig. 6d,e). TANGO2 did not enhance the transfer of free haem to apo-myoglobin (Extended Data Fig. 6f,g), indicating that it may facilitate the translocation of haem out of mitochondria.

TANGO2 proteins are unlikely to function as mitochondrial haem transporters because they are not predicted to contain transmembrane domains. By using mitochondria isolated from *TANGO2*-knockout cells, we demonstrated that externally-added TANGO2 protein was sufficient to stimulate the haem transfer (Extended Data Fig. 6h). Given that haem is an amphipathic molecule that can associate with membrane lipids[2], we used mitochondrial membranes as the haem donor and found that TANGO2 facilitated the transfer of haem associated with the membranes to apo-myoglobin (Fig. 5c). Furthermore, pre-treatment of the membranes with trypsin did not block the haem transfer (Extended Data Fig. 6i,j), implying that mitochondrial membrane proteins are not required for TANGO2-mediated haem transfer.

The N-terminal region of TANGO2 contains a cysteine and an NRDE motif that are highly conserved from yeast to humans (Fig. 5d). We examined whether these residues were

required for haem transfer by constructing TANGO2 lacking 13 or 28 amino acids at the N terminus. The haem transfer activity of TANGO2 was unaffected by removing its N-terminal 13 residues but was completely abolished by the deletion of its N-terminal 28 residues (Fig. 5e), indicating that the NRDE motif is critical for haem transfer.

TANGO2 binds haem

Recombinant TANGO2 protein displayed haem peroxidase activity after being incubated with haem (Extended Data Fig. 6f), indicating that TANGO2 binds haem. Analyses of Flag-tagged human and mouse TANGO2 proteins purified from mammalian cells verified this result (Fig. 5f,g). Similarly, recombinant yeast Tango2p also bound haem (Fig. 5h,i). Yeast Tango2p is more stable than mammalian TANGO2 proteins, making it feasible to evaluate the haem binding affinity. Titration of yeast Tango2p with haem revealed that it bound both ferrous haem and ferric haem with low affinity in vitro (Fig. 5j,k). The dissociation constants were estimated to be 15.4 μM for ferrous haem and 38.7 μM for ferric haem (Fig. 5j,k). Taken together, our results suggest that HRG-9 and TANGO2 proteins have a conserved role in trafficking haem from haem-enriched compartments in eukaryotic cells.

Discussion

Here we have identified HRG-9 and its homologue TANGO2 as evolutionarily conserved intracellular haem chaperones. In the haem auxotroph *C. elegans*, HRG-9 and its paralogue HRG-10 are required to mobilize haem out of the haem storage site LROs (Fig. 5l). In haem-synthesizing eukaryotes, the HRG-9 homologue TANGO2[14] facilitates haem transfer from mitochondria, the site of haem synthesis (Fig. 5l). HRG-9 and TANGO2 are likely to transfer haem from haem-enriched membranes independent of other haem-transporting proteins such as HRG-1, feline leukaemia virus subgroup C receptor 1b (FLVCR1b) and progesterone receptor membrane component 2 (PGRMC2)[10,25,26]. This mechanism partially resembles that of cytoplasmic lipid transfer proteins[27,28]. Haem, as a metal-containing lipid-like molecule[2], can intercalate into lipid membranes in a concentration-dependent manner[29]. TANGO2 has appreciably low affinity for haem, indicating that it acquires haem only from haem-enriched compartments. Mitochondria, the site of haem synthesis, are enriched in haem. For example, the yeast mitochondria contain more than 100 μM haem[30]. In the haem auxotroph *C. elegans*, the organelles with the highest haem content are LROs[18].

In humans, mutations in *TANGO2* cause an autosomal recessive inherited disease[4–8]. Individuals with *TANGO2* mutations manifest pleiotropic symptoms including encephalopathy, arrhythmias, rhabdomyolysis, lactic acidosis and hypoglycaemia[4–8]. We have shown that *TANGO2* deficiency impairs mitochondrial oxidative phosphorylation, providing a potential mechanism for the metabolic crisis in people with *TANGO2*-related disease. *tango2*$^{-/-}$ zebrafish larvae display encephalopathy, arrhythmia and myopathy, defects that partially resemble the symptoms of humans *TANGO2* deficiency. Thus, the identification of HRG-9 and TANGO2 as an intracellular haem chaperone provides a biological basis for exploring the aetiology and treatment of *TANGO2*-related disorders.

Methods

C. elegans culture and strains

Worms were maintained at 20 °C either on standard nematode growth medium (NGM) agar plates seeded with *Escherichia coli* or in liquid modified *C. elegans* habitation and reproduction (mCeHR2) medium[9]. *E. coli* strains OP50 and HT115(DE3) were used in this study.

N2 Bristol strain (wild-type) and RT130 (VIT-2::GFP)[15] *C. elegans* were obtained from the *Caenorhabditis*Genetics Center (CGC). IQ6011 (*hrg-1p::gfp*) was previously generated by the I. Hamza laboratory[10]. MGH41 (PGP-2::GFP) was obtained from the A. Soukas laboratory[17]. The following strains were generated in this study: CCH301 (*hrg-9(cck301)*V), CCH302 (*hrg-10(cck302)*V), CCH303 (*hrg-9(cck301)V; hrg-10(cck302)*V), CCH351 (cck351[*hrg-9p::nls-gfp*]), CCH352 (cck352[*hrg-10p::nls-gfp*]), CCH353 (cck353[*hrg-9p::hrg-9::gfp*]), CCH354 (cck354[*hrg-10p::hrg-10:: gfp*]), CCH304 (*hrg-9(cck301)*V; cck353[*hrg-9p::hrg-9::g fp*]), CCH305 (*hrg-10(cck302)*V; cck354[*hrg-10p::hrg-10::gfp*]), CCH306 (*hrg-9(cck301)*V; *hrg-10(cck302)*V; cck353[*hrg-9p::hrg-9::g fp*]), CCH307 (*hrg-9(cck301)*V; *hrg-10(cck302)*V; cck354[*hrg-10p::hrg-10:: g fp*]), CCH308 (*hrg-9(cck301)*V; IQ6011[*hrg-1p::g fp*]), CCH309 (*hrg-10(cck302)*V; IQ6011[*hrg-1p::gfp*]) and CCH310(*hrg-9(cck301)*V; *hrg-10(cck302)*V; IQ6011[*hrg-1p::gfp*]).

Zebrafish

Zebrafish experiments were approved by the Institutional Animal Ethics Committee of Zhejiang University. Zebrafish were maintained at 28 °C on a 14-h light/10-h dark cycle and manipulated using standard procedures. Wild-type AB line, *Tg(globin-LCR:EGFP)* transgenic line[31] and *tango2*$^{-/-}$ zebrafish were used in this study.

Yeast strains, plasmids, and growth conditions

S. cerevisiae strains used in this study were derived from BY4741 (*MAT*a, *his3*Δ1, *leu2*Δ0, *met15*Δ0, *ura3*Δ0). The *tango2*Δ::*kan*MX4 strain was obtained from the yeast gene deletion collection (Thermo Fisher Scientific) and confirmed by sequencing the unique barcodes flanking the *KanMX4* deletion cassette. The DH001–3b (*hem1*Δ::*HIS3*) strain was generated previously[19]. The *hap1Δ::URA* strains were generated using a PCR-based gene disruption strategy to replace the *HAP1* open reading frame (ORF) with the *URA3* marker. The pRS416 plasmid was used as a template to amplify the *URA3* gene flanked by 45 nucleotides of the 5′ and 3′ untranslated regions of *HAP1* using primers GAAATAGAAGAAAAAGAAAAAAAAAAAAAGGGAACAATAGGTTAGCTGTGCGG TATTTCACACCG and TTACATTATCAATCCTTGCGTTTCAGCTTCCACTAATTTAGATGAAGATTGTACTGA GAGTGCAC. The resulting deletion cassette was transformed into wild-type and *tango2Δ::kanMX4* strains.

Yeast transformations were performed using the lithium acetate procedure[32]. Strains were maintained at 30 °C on either enriched yeast extract–peptone-based medium supplemented

with 2% glucose (YPD), or synthetic complete (SC) medium supplemented with 2% glucose and the appropriate amino acids to maintain the selection. Culturing of *hem1*Δ cells required supplementing YPD or SC media with 50 μg ml^{-1} of 5-aminolevulinic acid or 15 mg ml^{-1} of ergosterol and 0.5% Tween-80 (YPDE or SCE, respectively)[19,33]. All liquid cultures were maintained at 30 °C and shaken at 220 rpm.

Cytosolic, mitochondrial, and nuclear-targeted haem sensors, HS1 and HS1(M7A), were sub-cloned into pRS415 and driven by the GPD promoter as previously described[19,22]. The Hap1 reporter plasmid in which EGFP is driven by the *CYC1* promoter has also been previously described[19,22].

Mammalian cell lines and culture conditions

HEK293 cells were cultured in Dulbecco's modified Eagle's medium (DMEM) with 10% fetal bovine serum (FBS), 1% 100× penicillin-streptomycin at 37 °C with 5% CO_2. To inhibit haem synthesis, cells were incubated with 0.5 mM succinylacetone for 24 h. MEL cells were maintained in DMEM supplemented with 10% FBS, 1% penicillin-streptomycin, 1% sodium pyruvate, 1% glutamine and 1% non-essential amino acid mix. Erythroid-like differentiation of MEL cells was induced by supplementing 1.5% dimethyl sulfoxide (DMSO).

Extraction and quantification of haem

Worms, zebrafish embryos and mammalian cells were lysed with ~10 pellet volumes of 1 M HCl and haem was extracted with equal volume of 2-butanone. Following evaporation of 2-butanone, the haem pellet was resuspended in DMSO. Aliquots of the worm and cell samples were used to measure the protein concentration using BCA protein assay kit (Beyotime). Yeast cells were treated with 20 mM oxalic acid and stored at 4 °C for 16–18 h to extract haem following the method described[22].

Haem from equal amount of proteins or equal number of cells was quantified by fluorescence porphyrin assays[34]. In brief, 2 M oxalic acid was added to each sample, and the sample was split into 2 equivalents. One half was heated to 95 °C for 30 min to release iron from haem, while the other half was kept at 25 °C. The suspensions were centrifuged to remove debris prior to measurement of porphyrin fluorescence on a Synergy H1 or a Synergy Mx plate reader (excitation: 400 nm; emission: 608 nm). Haem concentration in each well was calculated against a standard curve prepared with series dilutions of haemin chloride. The values of unheated samples were subtracted from those of the corresponding heated samples. For worms, zebrafish embryos and mammalian cells, the concentrations of haem were normalized to protein concentrations. For non-mitochondrial fractions, the concentration of BSA (2 mg ml^{-1}) added to the cell lysis buffer was subtracted prior to calculation. For yeast, the concentration of haem was determined by dividing the moles of haem by the number of cells analysed, and then converting to a cellular concentration by dividing by the volume of a yeast cell, taken to be 50 fl[19].

o-dianisidine staining

Haemoglobin in MEL cells and zebrafish embryos was stained with *o*-dianisidine following the described method[35]. MEL cells were stained with *o*-dianisidine (0.68 mM *o*-dianisidine, 14 mM acetic acid, 73 mM H_2O_2) at day 3 after DMSO-induced differentiation. Zebrafish embryos were stained with *o*-dianisidine (2.54 mM *o*-dianisidine, 11 mM sodium acetate, 0.22 M H_2O_2) at 48 and 72 h post-fertilization (hpf). The stained samples were analysed with an Olympus IX73 microscope or Leica M165 FC microscope connected to a Leica DFC310 FX camera. Images were acquired and processed using LAS software (Leica).

RNA extraction and RT–qPCR

Total RNA was extracted using TRIzol (Invitrogen). After treatment with RQ1 RNase-Free DNase (Promega), RNA was reverse transcribed using the TransScript First-Strand cDNA Synthesis Kit (Transgen). RT–qPCR was performed in triplicate using the ChamQ SYBR quantitative PCR reagent (Vazyme) in a CFX96 Real-Time PCR system (Bio-Rad). The data were acquired and processed using CFX Manger (Bio-Rad). The expression of genes was normalized to worm *gpd-2* or zebrafish *gapdh* by the $\Delta\Delta C_t$ method. The primers used for quantitative PCR are as follows: worm *gpd-2* (forward, TGCTCACGAGGGAGACTAC; reverse, CGGTGGACTCAACGACATAG), *hrg-1* (forward, AATGGCAGGATGGTCAGAAAC; reverse, CGATGAATGAAAGGAACGATACG), *hrg-9* (forward, GTAGAGGAGGAATAGTGAACGAG; reverse, CTTCAGTTGACAAACTTCAATTTCGTC), *hrg-10* (forward, GAACAATAGAGATGAGGATTTGGACC; reverse, CTTTTCCATGTGCATCCATTCCTAGC), zebrafish *gapdh* (forward, CAAGGCTGTAGGCAAAGTAATTC; reverse, CTTGATCTCATCATACTTGGCAG), zebrafish *c-fos* (forward, GACAGCGTCGGGTATTACCC; reverse, CATCCACTGCAAGTCCGGGC).

Generation of knockout and transgenic worm strains

C. elegans hrg-9 and *hrg-10* were knocked out using CRISPR–Cas9 technology. Two guide RNAs (gRNAs) targeting the first exon of *hrg-9* (GCAACTTCTTCGGCCAACAA and AAGGAAATGCATTGGCATGA) and two guide RNAs targeting the first and last exons of *hrg-10* (ACTCCCATTCACTGGCACGA and CATGGAGCCTGCGGAGAGCG) were cloned into a modified pDD162 vector[36,37]. The gRNA plasmids were injected together with the dpy-10 co-CRISPR plasmid[38] into adult N2 worms. Deletion was screened by PCR genotyping with the following primers: *hrg-9* (forward, CATATGACGCAATTTTGTGGTCATTC; reverse, GACTCTATCATTTTCGAAGTATCATTAGC), *hrg-10* (forward, CCAGAGTTTTCCAAAATGTGCATTG; reverse 1, GAATTCAAATTTCTTAATGAACAGTGTCTG; reverse 2, CCCCAAGTTTTAGTGCATTTTTGAG). The derived alleles *hrg-9(cck301)* and *hrg-10(cck302)* were verified by sequencing, and the mutants were outcrossed four times with N2 worms.

To construct the transcriptional reporters (*hrg-9p::nls-gfp* and *hrg-10p::nls-gfp*), the *hrg-9* promoter (821 bp upstream of *hrg-9* start codon) and the *hrg-10* promoter (1172 bp

upstream of *hrg-10* start codon) were amplified from genomic DNA and inserted into pPD95.67 (Addgene). For construction of translational reporters (*hrg-9p::HRG-9::GFP* and *hrg-10p::HRG-10::GFP*), the promoters along with their own genes were cloned into pPD95.75 (Addgene). To ectopically express *TANGO2* genes in the worm, the ORFs of human *TANGO2* (NM_152906.7), zebrafish *tango2* (NM_001003781.1) and yeast *tango2* (NM_001181256.1) were subjected to codon optimization to facilitate their expression in *C. elegans*. Two to seven artificial introns were inserted into each gene, and the products were cloned into pPD95.75 with the *hrg-10* promoter. The transgenes were introduced into worms by microinjection and integrated into the genome with trimethylpsoralen and ultraviolet light.

RNAi in the worm

Open reading frames of target genes were cloned into the L4440 vector (Addgene). RNAi plates were prepared by adding 2 mM isopropyl-β-d-thiogalactopyranoside (IPTG), 50 μg ml^{-1} carbenicillin and 12 μg ml^{-1} tetracycline to the NGM recipe and seeding with HT115(DE3) *E. coli* carrying empty vector or L4440 plasmids. Synchronized L1 worms were cultured on RNAi plates for 3 days followed by phenotypic examination.

Transcriptome sequencing of *C. elegans* intestines

Haem-regulated genes in the *C. elegans* intestine were analysed using SMART-Seq technology following a previously described protocol[39]. Synchronized worms were cultured in mCeHR2 medium with 2 μM, 20 μM, or 400 μM haem for one generation. The adult worms were paralysed with 0.5 mM levamisole and cut right behind the pharynx using a needle following the procedure described previously[40]. The extruded intestines were immediately transferred to a hypotonic lysis buffer (0.2% Triton X-100) supplemented with RNase inhibitor (Vazyme). Intestines from three adult worms were combined into one sample to minimize the sample variability. Following the lysis of intestinal cells, reverse transcription was performed with SMARTScribe Reverse Transcriptase (Takara Bio), an oligo(dT) primer containing the adapter sequence, and a template-switching oligonucleotide (TSO)[39]. The reverse transcriptase adds a few non-template nucleotides to the end of the newly synthesized cDNA, which can base pair with the matching sequence in the TSO. The reverse transcriptase then switches the template to TSO and adds an adapter sequence to the end of the cDNA. After reverse transcription, the cDNA was amplified by PCR.

The sequencing library was constructed according to the manufacturer's instructions (Illumina) and sequenced on the Illumina NovaSeq 6000 platform (2 × 150 bp). The reads were mapped to *C. elegans* reference genome by HISAT[41], followed by assembling into genes using StringTie[42]. Fragments per kilobase of transcript per million mapped reads (FPKM) were calculated by StringTie[42]. The FPKM values in the groups treated with 2 μM and 400 μM haem were compared with those in the group of 20 μM haem using EdgeR[43].

Worm imaging

Worms were paralysed in 10 mM levamisole and imaged as described previously[37]. To assess the intensity of GFP fluorescence, 6–7 worms of the same group were placed onto a single slide and imaged using an Olympus IX73 epifluorescence microscope with LAS

software (Leica). The GFP images shown within each figure panel were collected using the same acquisition setting. GFP fluorescence was quantified using ImageJ software (National Institutes of Health). To examine the spatial expression and subcellular localization, GFP and differential interference contrast (DIC) images were obtained using Zeiss LSM710 confocal microscope and processed using ZEN software (Zeiss). To monitor the worm growth and lethality, brightfield images were collected using the Olympus IX73 microscope with LAS software (Leica).

ZnMP labelling and chasing in the worm

ZnMP (Frontier Scientific) was prepared following the procedure described previously[9]. For ZnMP staining, L4-stage worms were cultured in axenic mCeHR2 medium containing 40 μM ZnMP and 4 μM haem at 20 °C for 16 h. The stained worms were washed extensively with M9 salt buffer followed by fluorescence analysis with the Olympus IX73 microscope. To measure the ZnMP uptake kinetics, L4-stage worms were stained with 40 μM ZnMP for 0, 2, 4, 6 or 8 h followed by imaging. For ZnMP chasing experiments, L4-stage worms were labelled with 40 μM ZnMP in CeHR2 medium for 12 h. The worms were then incubated in fresh mCeHR2 medium supplemented with 200 μM haem for 0, 4, 8, 12, 16 or 24 h prior to imaging analysis. Images were acquired using LAS software (Leica) and the intensity of ZnMP was quantified using ImageJ software (National Institutes of Health).

To determine whether ZnMP colocalizes with LROs, the PGP-2::GFP transgenic worms were cultured on RNAi plates followed by ZnMP staining. To examine the colocalization between ZnMP and LysoSensor, worms were cultured on NGM plates containing 50 μM LysoSensor Green (Invitrogen) for 30 min following ZnMP staining. The stained worms were transferred to regular NGM plates to clear LysoSensor from the intestinal lumen for 1.5 h. The stained worms were analysed using LSM710 confocal microscope with ZEN software (Zeiss).

GaPP toxicity assay in the worm

Gravid worms (P_0) were placed on NGM plates containing 0.5 μM or 1 μM GaPP (Frontier Scientific) to lay eggs. After 6–8 h, the P_0 worms were removed. The growth and survival of the F_1 progeny on the GaPP-containing NGM plates were examined after 3–4 days. Worms were scored as dead if they did not respond to prodding. The GaPP toxicity assays were performed in triplicates, and at least 50 worms were analysed for each sample.

^{15}N-haem uptake in the worm

^{15}N-labelled haem was generated in MEL cells by culturing them with 4 mM ^{15}N-glycine (Shanghai Research Institute of Chemical Industry) and 1.5% DMSO for 3 days. Haem was extracted from the cells and analysed by high-performance liquid chromatography–mass spectrometry (HPLC–MS) on a LCD Deca XP MAX mass spectrometer (Thermo Electron Corporation) connected to an Agilent 1200 HPLC instrument (Agilent). The labelling efficiency of the ^{15}N-haem produced by MEL cells was found to be ~82%. Synchronized L1-stage worms were cultured in mCeHR2 medium with 4 μM haem till young adult stage. The young adult worms were incubated in mCeHR2 medium containing 4 μM ^{15}N-haem for 3 h. Wild-type worms cultured with high (200 μM) haem, which is known to downregulate

the haem uptake, were used as control. Total haem was extracted from worms with 1 M HCl and 2-butanone and analysed by HPLC–MS as described above. The peak area of ^{15}N-haem, as well as the ratio of ^{15}N-haem to ^{14}N-haem, was normalized to the protein concentration.

Knockout of *tango2* in zebrafish

Tango2-knockout zebrafish was generated by CRISPR–Cas9 technology following the method described previously[44]. Two gRNAs (gRNA1: AGACTGGATGCGCTAGGTGC; gRNA2: GGAGCTACTAATGTACCTGT) targeting the second exon of *tango2* (NM_001003781.1) were used. The mutant animals were screened and genotyped using two primers (forward, TAACTCACTGTCACATCTCTTC; reverse, GCATGATTCAGCATCCACTGGAC). Following sequencing verification, the knockout efficiency was further confirmed at the RNA level by reverse transcription PCR using the primers (forward, ATGTGCATCATCTTCTTGAAGTTCGACC; reverse, GCATGATTCAGCATCCACTGGAC and GGGGTGTTTAGCTCCTCGTTATTG).

Whole-mount in situ hybridization of zebrafish embryos

Whole-mount in situ hybridization was carried out with digoxigenin-labelled probes following a previously described protocol[45]. The expression of *tango2* was analysed in wild-type zebrafish embryos at 1-cell and 1,000-cell stages and 24 hpf. The erythroid markers *gata1a* and *αe3-globin* were analysed in wild-type and *tango2*-knockout embryos at 24 hpf and 48 hpf, respectively.

Quantification of erythrocytes in *Tg(globin-LCR:EGFP)* zebrafish embryos

The *tango2* mutant was crossed with the *Tg(globin-LCR:EGFP)* transgenic line. Single-cell suspensions were prepared from wild-type and *tango2*-knockout transgenic embryos at 24–72 hpf, following a procedure described previously[35]. The percentage of GFP-positive cells was analysed using the CytoFLEX LX Flow Cytometer with CytExpert software (Beckman).

Zebrafish locomotor activity assay

The locomotor activity of zebrafish larvae was monitored using the DanioVision observation chamber with EthoVision XT software (Noldus). Zebrafish larvae at 12 dpf were placed into 24-well plates (one larva per well). After acclimation for 1 h, the movement of larvae was recorded for 40 min either in constant dark or in 10 min light-dark cycles.

Micro-CT analysis of zebrafish brain

Zebrafish larvae at 12 dpf were fixed with 4% paraformaldehyde and stained with 0.3% phosphotungstic acid (Sigma-Aldrich). The head regions were analysed using Skyscan 1272 Control Program on a Skyscan 1272 high-resolution micro-CT scanner (Bruker) with the parameter of 1 μm/pixel, 50 kV, 65 μA, and 0.2° rotation step. The images were reconstructed using the NRecon Reconstruction software (Bruker) and analysed using the DragonFly software (Object Research Systems).

Zebrafish heartbeat recording

Zebrafish larvae at 12 dpf were partially immobilized in an E3 buffer containing 2% methylcellulose. The heart beats were recorded on a Nikon SMZ745T microscope equipped with an OPLENIC Pro microscope camera for 1 min. The heart rate was calculated as beats per minute.

Analysis of cardiac rhythm in zebrafish larvae

Zebrafish embryos were treated with *N*-phenylthiourea from 24 hpf to prevent pigmentation. Zebrafish larvae at 7 dpf were paralysed with 0.16 mg ml^{-1} Tricaine (Sigma-Aldrich) and immobilized in E3 buffer containing 2% methylcellulose. The heart contractions were recorded using NIS-Elements software on a Nikon SMZ18 microscope and quantified using the Changing Pixel Intensity Algorithm in the Semi-Automated Optical Heartbeat Analysis (SOHA) software[46]. The heart period, systolic interval, and diastolic interval were calculated by the SOHA software following the method described[46]. The arrhythmicity index was calculated as the ratio of the standard deviation of heart period to the median heart period[46].

Histological analysis of zebrafish muscle

Zebrafish larvae were fixed with 4% paraformaldehyde and dehydrated with increasing concentrations of ethanol. After embedding in paraffin, tissues were sectioned to 3-μm thickness and were stained with haematoxylin and eosin. Images were acquired on an Olympus IX73 microscope with LAS software (Leica).

Birefringence assay and whole-mount phalloidin staining of zebrafish muscle

The birefringence of zebrafish muscle was analysed following a previous method[47]. In brief, the anaesthetized larvae were placed on a polarizing filter and subsequently covered with a second polarizing filter. The filters were placed on an Olympus IX83 microscope. The polarizing filter on the top was twisted until only the light refracted through the striated muscle was visible. Images were acquired using cellSens Dimension 2.3 software (Olympus).

Zebrafish larvae were fixed with 4% paraformaldehyde, permeabilized with 50 μg ml^{-1} proteinase K, and stained with 0.5% phalloidin (Bioscience). The stained samples were analysed using LAS X software (Leica) on a Leica TCS SP8 STED microscope.

Yeast growth test

Growth tests of wild-type, *hem1*Δ and *tango2*Δ cells were performed by growing 10-ml cultures for 14–16 h to mid-exponential phase. Cultures were then diluted to 0.2 A_{600} units per ml 50-ml cultures in SC media supplemented with or without 400 μg ml^{-1} ALA. Cultures were grown for 16 h and OD_{600} readings were taken every hour for 16 h using a Cary 60 UV/vis spectrophotometer (Agilent).

Steady-state labile haem measurements in the yeast

To measure steady-state labile haem, wild-type, *hem1*Δ, and *tango2*Δ cells expressing the HS1-M7A haem sensors were cultured in 10 ml SCE-LEU media, with or without 0.5

mM succinylacetone, for ~14–16 h to mid-exponential phase (A_{600} ≈ 1–2). Cytosolic and mitochondrial-targeted sensors were expressed on low copy centromeric plasmids and were driven by the GPD promoter (p415-GPD)[19,22]. After culturing, cells were collected, washed in water, and resuspended in phosphate buffered saline (PBS) solution to a density of 10 A_{600} units per ml. Two-hundred mirolitres of the cell suspension, corresponding to 2 A_{600} units or 4 × 10^7 cells, was used to measure EGFP (excitation 488 nm, emission 510 nm) and mKATE2 (excitation 588, emission 620) HS1-M7A sensor fluorescence. Background autofluorescence of cells not expressing the sensors was recorded and subtracted from the EGFP and mKATE2 sensor fluorescence values. Fluorescence was recorded on a Synergy Mx multi-modal plate reader using black Greiner Bio-one flat bottom fluorescence plates.

Haem trafficking dynamics assay in the yeast

Inter-compartmental haem trafficking rates were monitored as described[22]. In brief, HS1-expressing cells were cultured with or without 500 μM succinylacetone (Sigma-Aldrich) in SCE-LEU medium. Triplicate 5-ml cultures were seeded at an initial density of 0.01–0.03 A_{600} units per ml (2–6 × 10^5 cells per ml) and grown for 14–16 h at 30 °C, with or without 500 μM succinylacetone (Sigma-Aldrich) in SCE-LEU medium, shaking at 220 rpm until cells reached a final density with A_{600} approximately 1.0 (2 × 10^7 cells per ml). After culturing, 1 absorbance unit (~2 × 10^7 cells) of cells were collected, washed twice with 1 ml sterile ultrapure water, and resuspended in 1 ml fresh SC-LEU medium. The cells that were pre-cultured without succinylacetone provided reference values for EGFP/mKATE2 fluorescence ratios associated with maximal haem loading of HS1 (R_{max} values). The succinylacetone-conditioned cells were split into two 500 μl fractions. One fraction was treated with 500 μM succinylacetone to give EGFP/mKATE2 fluorescence ratios associated with minimal haem loading of HS1 (R_{min} values). The other fraction was not treated with succinylacetone so that haem synthesis could be re-initiated to give compartment-specific haem trafficking rates. HS1 fluorescence was monitored using 200 μl of 1 A_{600} unit per ml (2 × 10^7 cells per ml) cell suspension in black Greiner Bio-one flat bottom fluorescence plates with a Synergy Mx multi-modal plate reader. EGFP (excitation 488 nm, emission 510 nm) and mKATE2 (excitation 588 nm, emission 620 nm) fluorescence was recorded every 5 min for 4 h, with the plate being shaken at medium strength for 30 s prior to each read. Background fluorescence of cells not expressing the haem sensors was recorded and subtracted from the EGFP and mKATE2 fluorescence values. The fractional haem saturation of the sensor was determined using the following equation: sensor bound (%) = $(R - R_{min})/(R_{max} - R_{min})$.

Analysis of the p415–CYC1–EGFP reporter activity in the yeast

Wild-type, *tango2*Δ, *hap1*Δ and *hap1*Δ*;tango2*Δ yeast strains expressing p415–CYC1–EGFP were cultured in 10 ml SCE-LEU media for ~14–16 h to a density of 1–2 A_{600} units per ml. Cells were resuspended in PBS to a concentration of 10 A_{600} units per ml and 200 μl (2 A_{600} units or 4 × 10^7 cells) was used to measure EGFP fluorescence (excitation 488 nm, emission 510 nm). Background autofluorescence of cells not expressing EGFP was recorded and subtracted from the EGFP-expressing strains.

Measurement of catalase expression and activity in the yeast

The expression and activity of yeast catalase were measured following the methods described previously[48,49]. In brief, yeast cells were cultured in 10 mL SCE media for 14–16 h to mid-exponential phase. Cells were lysed using zirconium oxide beads in a Bullet Blender (Next Advance)[19]. Protein concentrations were determined by the Bradford method (Bio-Rad) and 100 μg protein were subjected to SDS–PAGE on 10% Tris-glycine gels (Invitrogen). Following incubation with anti-Ctt1p[50] or anti-GAPDH (Genetex) primary antibodies and a goat anti-rabbit secondary antibody conjugated to a 680 nm emitting fluorophore (Biotium), the blots were imaged on a LI-COR Odyssey Infrared imager[19].

To detect the catalase activity, 15 μg protein lysates were analysed by PAGE on a 10% Tris-glycine gel (Invitrogen). After electrophoresis, an in-gel activity stain was utilized to measure catalase activity[48,51]. In brief, the catalase staining solution was prepared by mixing 1 part dopamine (20 mg ml^{-1}) and 1 part para-phenylenediamine (3.5 mg ml^{-1}) in 0.2 M potassium phosphate buffer, pH 8, 1 part 15% H_2O_2, and 2 parts DMSO in the order listed. The staining solution was added directly to the gel and allowed to stain for 2 min, followed by imaging.

Knockout of *TANGO2* in HEK293 and MEL cells

TANGO2-knockout HEK293 cells and *Tango2*-knockout MEL cells were generated with CRISPR–Cas9 technology[52]. Guide RNAs targeting the second and ninth exons of human *TANGO2* (CTCTGCTGACACAGGTCGCG and CGTGGCCGTCCGCATCTACC) and the third and ninth exons of mouse *Tango2* (GCCCTTGTTCTGCCTCCGCC and CCTGAAGGGCCAGCGTGGAC) were cloned into the pX330 vector (Addgene). The gRNA plasmids together with a modified pEF1α plasmid[44], which encodes a puromycin-resistance gene, were electroporated into HEK293 cells and MEL cells using the Gene Pulser Xcell Electroporation System (Bio-Rad). The transfected cells were selected with 5 μg ml^{-1} puromycin for 7–10 days. Cell clones were screened for knockout by genotyping with the following primers and verified by immunoblotting analysis. Human *TANGO2*: forward, GCCAAGAGTGTGGTGTCCAGTTC; reverse 1, CAAGCTGGCTCTCACTCACTGAC; reverse 2, GCAGTGCAATGCAGTATGGCAAAG. Mouse *Tango2*: forward, GAGAGAGACATCCGAAAAGCCC; reverse 1, GCAGCAGTAGTAGGACTCTCC; reverse 2, CAAACAGGTCTGTGTGTTCACATAC.

Measurement of OCR

The OCR was measured using the Seahorse XF96 Analyzer with Wave Controller Software (Agilent Technologies). Equal number of cells were seeded in XF96 plates and equilibrated in the XF medium (Agilent Technologies). The OCRs were measured under basal conditions and following consecutive treatments of oligomycin (1.5 μM), FCCP (1 μM), and rotenone (0.5 μM) + antimycin A (0.5 μM).

Measurements of mitochondrial membrane potential and ATP concentration

The mitochondrial membrane potential was determined with TMRE (Thermo Fisher Scientific). Following the TMRE staining, the cells were analysed by both flow cytometry

and confocal microscopy. The mean fluorescence intensity of TMRE was determined using CytoFLEX LX Flow Cytometer with CytExpert software (Beckman). TMRE fluorescence images were acquired on a LSM710 confocal microscope with ZEN software (Zeiss).

The ATP concentration was measured by the luciferin–luciferase assay with an enhanced ATP Assay Kit (Beyotime). The values were normalized to the protein concentration.

Immunofluorescence assays in mammalian cells

HEK293 cells seeded on glass coverslips were transfected with a TANGO2–Flag construct. After 48 h, the cells were fixed in 4% paraformaldehyde, incubated with a mouse anti-Flag antibody (Sigma-Aldrich) and a rabbit anti-COX IV (Abcam), followed by incubation with a goat anti-rabbit antibody conjugated to Alexa 568 and a goat anti-mouse antibody conjugated to Alexa 488 (Thermo Fisher Scientific). Fluorescence images were acquired on a LSM710 confocal microscope with ZEN software (Zeiss).

Immunoblotting

Proteins in individual samples were resolved on 10% or 12% SDS–PAGE gels and transferred onto nitrocellulose membranes (Bio-Rad). Following incubation with primary antibodies and HRP-conjugated secondary antibodies, the membranes were developed with enhanced chemiluminescence substrates (Thermo Fisher Scientific) in the XRS+ Gel documentation system (Bio-Rad) with Image Lab Software (Bio-Rad). Antibodies used in this study are anti-TANGO2 (Proteintech), anti-COX IV (Abcam), anti-GAPDH (Genetex, for yeast), anti-GAPDH (Santa Cruz, for mammalian cells), anti-β-actin (Huabio) and anti-Ctt1p (generated by the laboratory of A.R.R.).

Isolation of mitochondria and mitochondrial membranes from mammalian cells

Mouse experiments were approved by the Institutional Animal Ethics Committee of Zhejiang University. HEK293 cells, MEL cells, and mouse liver cells were homogenized in a MS buffer (210 mM mannitol, 70 mM sucrose, 20 mM HEPES, pH 7.4) supplemented with 2 mg ml^{-1} BSA and Protease Inhibitor Cocktail (1:100, Sigma-Aldrich). The homogenates were centrifuged at 800 *g* for 10 min at 4 °C to remove nuclei and cell debris. The post-nuclear supernatants were further centrifuged at 12,000 *g* for 10 min at 4 °C to pellet mitochondria. The mitochondrial pellets were washed twice with MS buffer for further analysis.

To prepare mitochondrial membranes, the mitochondria isolated from mouse liver cells were disrupted in a buffer containing 100 mM KCl, 250 mM sorbitol, 50 mM HEPES, pH 7.4, and Protease Inhibitor Cocktail (1:100, Sigma-Aldrich). The homogenates were centrifuged at 12,000 *g* for 15 min at 4 °C to remove unbroken mitochondria. The supernatants were further centrifuged at 100,000 *g* at 4 °C for 1 h to precipitate the mitochondrial membranes. To prepare protein-free membranes, the isolated mitochondrial membranes were treated with 0.25% trypsin for 1 h at 37 °C, followed by washing extensively with a buffer (225 mM sucrose, 5 mM $MgCl_2$, 5 mM succinate, 10 mM KCl, 10 mM HEPES, pH 7.4).

Recombinant protein expression and purification

Open reading frames of human *TANGO2* (NM_152906.7), zebrafish *tango2* (NM_001003781.1), yeast *Tango2p* (NM_001181256.1), and the N-terminal truncated human *TANGO2* (ΔN13 and ΔN28) were cloned into the pET-28a vector (Addgene). The constructs were transformed into the BL21(DE3) *E. coli*. Expression of the recombinant genes were induced by culturing the bacteria with 0.2 mM IPTG at 18 °C for 12 h. The cells were lysed by sonication in a lysis buffer (500 mM NaCl and 20 mM Tris-HCl, pH 7.9) supplemented with 1 mM phenylmethylsulphonyl fluoride (PMSF). After centrifugation at 16,000 g at 4 °C for 10 min, the supernatant was filtered through a 0.45 μm filter and loaded onto a Ni^{2+}-charged histidine-binding column (Novagen). After washing with the lysis buffer containing 50 mM imidazole, the bound proteins were eluted with 500 mM imidazole. The eluates were dialysed against cold lysis buffer in a dialysis bag with molecular weight cut-off of 10 kDa. Aliquots of the purified proteins were analysed by BCA protein concentration assay and SDS–PAGE.

Purification of Flag-tagged mammalian TANGO2

The open reading frames of human *TANGO2* (NM_152906.7) and mouse *Tango2* (NM_138583.2) were cloned into a modified pEF1α plasmid[44]. HEK293 clones and MEL clones stably expressing TANGO2–Flag were generated by electroporation followed by puromycin selection. TANGO2–Flag was purified from the lysates of stable clones using anti-Flag M2 Affinity Gel (Sigma-Aldrich) as previously described[53].

Haem staining by chemiluminescence

Peroxidase activity of protein-associated haem was assayed following a method described previously[54]. The purified proteins, haem binding reactions, or haem transfer reactions were mixed with a sample buffer with no reducing agent. The samples were analysed by SDS–PAGE without heating. After transferring the proteins from gels onto nitrocellulose membranes (Bio-Rad), the peroxidase activity of haem was detected using the enhanced chemiluminescence (ECL) kit (Thermo Fisher Scientific) on the ChemiDoc XRS+ system (Bio-Rad) with Image Lab Software (Bio-Rad). In parallel to the haem activity assay, another gel with the same samples was prepared and stained with Coomassie blue to visualize the proteins.

Haem binding assay

Haemin was freshly dissolved in DMSO prior to each experiment. To set up the haem binding assay, 10 μM haemin was incubated with 10 μM protein in the binding buffer (150 mM NaCl, 50 mM Tris-HCl, pH 7.9) at 20 °C for 1 h in the dark. Sodium dithionite (10 mM) was used to reduce ferric haemin to ferrous haem. Absorption spectra were detected using the UV-2700 UV-vis spectrophotometer (Shimadzu). The binding reaction was also subjected to chemiluminescence haem staining to visualize the association of haem to proteins.

To measure the affinity of yeast Tango2p for haem, 10 μM protein was incubated with increasing concentrations (0.5–30 μM) of haemin in the presence or absence of sodium dithionite. Corresponding concentrations of haem were used as references. Differential

spectra were obtained by subtracting the absorbance values of haem references from those of the binding reactions. The K_d was determined with the differential absorbance values at 419 nm (ferric) or 414 nm (ferrous) by nonlinear curve fitting using GraphPad Prism.

In vitro haem transfer assay

The haem transfer experiment was modified from a previous method[55]. The purified mitochondria, mitochondrial membrane fractions, or haem were used as haem donor, and apo-myoglobin was used as a haem acceptor. The HEK293 cells used for this study were incubated with 50 μM haemin for 2 h prior to the isolation of mitochondria. Apo-myoglobin was generated by stripping haem off the myoglobin (Sigma-Aldrich) using the acid–butanone method. Haem transfer was assayed in a reaction buffer (225 mM sucrose, 5 mM $MgCl_2$, 5 mM succinate, 10 mM KCl, 10 mM HEPES, pH 7.4) by incubating the haem donor with 5 μM apo-myoglobin the presence or absence of 3 μM purified protein. The haem transfer activities were assayed for human TANGO2, TANGO2(ΔN13), TANGO2(ΔN28), zebrafish Tango2, yeast Tango2p, BSA, and GFP. After incubation at 37 °C for 2 h, the reaction was centrifuged at 12,000 *g* for 10 min at 4 °C to remove mitochondria or at 100,000 *g* for 1 h at 4 °C to remove mitochondrial membranes. The resultant supernatants were subjected to haem activity assay and Coomassie staining.

Statistics and reproducibility

Data are presented as mean ± s.e.m. Statistical analyses were performed using Prism 7 (GraphPad Software). Statistical significance was determined by one-way analysis of variance (ANOVA) followed by Tukey's multiple comparisons. A P value of < 0.05 was considered statistically significant. All experiments (except for the RNA-seq experiment, which was done once) were performed at least two times with similar results. No statistical method was used to predetermine sample size.

Extended Data

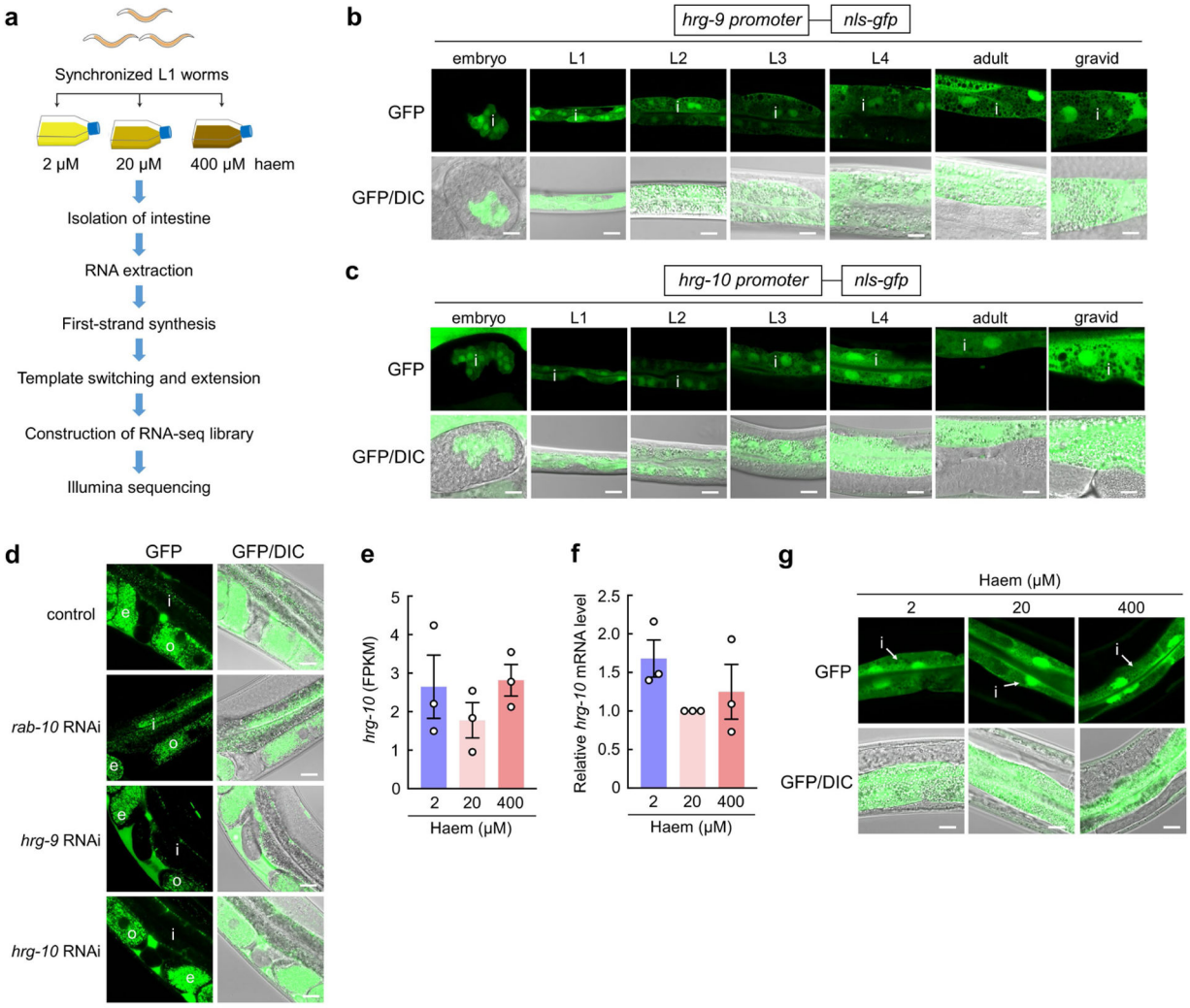

Extended Data Fig. 1 |. Analysis of *hrg-9* and *hrg-10* expression in *C. elegans*.

a, Workflow of RNA sequencing experiment. Synchronized L1 worms were grown in mCeHR2 medium containing 2 μM, 20 μM, or 400 μM haem to the gravid stage, and the intestines were isolated for transcriptomics analysis using the SMART-Seq technology. **b**, The *hrg-9p::nls-gfp* transcriptional reporter is expressed in the intestine of *C. elegans* at all developmental stages. nls, nuclear localization signal; i, intestine. Scale bars, 20 μm. **c**, The *hrg10p::nls-gfp* transcriptional reporter is predominantly expressed in the intestine of *C. elegans* at all developmental stages. nls, nuclear localization signal; i, intestine. Scale bars, 20 μm. **d**, Knockdown of *hrg-9* and *hrg-10* by RNAi does not impair the intestinal secretion of YP170::GFP in *C. elegans*. The known trafficking gene *rab-10* is used as a control. i, intestine; o, oocyte; e, embryo. Scale bars, 20 μm. **e**, RNA-seq demonstrates that intestinal *hrg-10* expression is not significantly affected by haem levels in *C. elegans*. n = 3 independent samples for each group. **f**, Quantitative RT-PCR shows that haem does not regulate *hrg-10* expression at the organismal level in *C. elegans*. n = 3 independent experiments. **g**, Haem does not regulate the expression of *hrg-10p::nls-gfp* transcriptional

reporter. Scale bars, 20 μm. Data in **e** and **f** are presented as mean ± s.e.m. Statistical significance was determined by one-way ANOVA followed by Tukey's test.

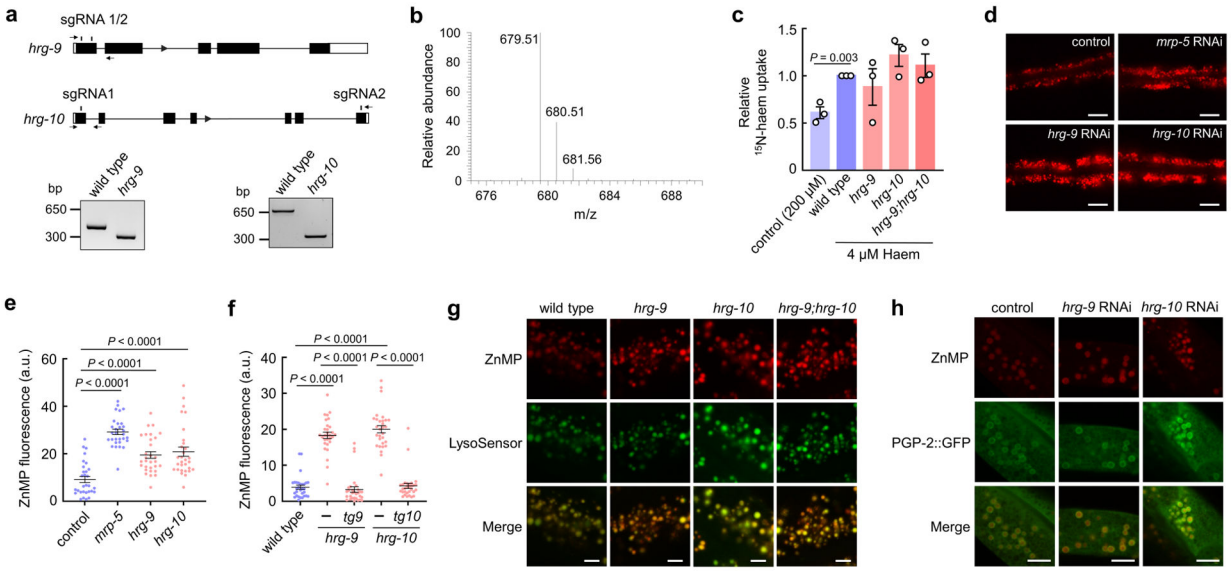

Extended Data Fig. 2 |. *hrg-9* and *hrg-10* regulate haem homeostasis in *C. elegans*.
a, Knockout of *hrg-9* and *hrg-10* in *C. elegans*. The sgRNA targeting sites and the positions of genotyping primers (arrows) are shown in the knockout strategies (top), and the genotyping results are shown at the bottom. **b**, Representative raw mass spectra of ^{15}N-haem and ^{14}N-haem mixture from *C. elegans*. The ^{14}N-haem shows a mass to charge ratio (m/z) of 679.51 and the ^{15}N-haem shows m/z of 680.51 and 681.56. **c**, The uptake of ^{15}N-haem in *hrg-9* and *hrg-10* knockout worms is comparable to that of wild type worms. Worms were incubated with 4 μM ^{15}N-haem for 3 h, and the total haem in worms were extracted for analysis by mass spectrometry. Wild type worms cultured with 200 μM haem were used as a control. n = 3 independent experiments. **d**,**e**, Representative images (**d**) and quantification (**e**) of zinc mesoporphyrin IX (ZnMP) staining in worms treated with control, *mrp-5*, *hrg-9*, or *hrg-10* RNAi. The known haem transporter *mrp-5* is used as a control. n = 30 worms examined over 3 independent experiments. Scale bars, 20 μm. **f**, The ZnMP accumulation phenotypes in *hrg-9* and *hrg-10* knockout worms are rescued by the expression of HRG-9::GFP and HRG-10::GFP, respectively. tg9, HRG-9::GFP; tg10, HRG-10::GFP. n = 30 worms examined over 3 independent experiments. **g**, Wild type, *hrg-9*, *hrg-10*, and *hrg-9;hrg-10* adults were stained with ZnMP and LysoSensor Green. Scale bars, 5 μm. **h**, ZnMP colocalizes with PGP-2::GFP, a marker of lysosome-related organelles, in control, *hrg-9*, and *hrg-10* RNAi worms. Scale bars, 10 μm. Data in **c**,**e**,**f** are presented as mean ± s.e.m. *P* values were determined by one-way ANOVA followed by Tukey's test.

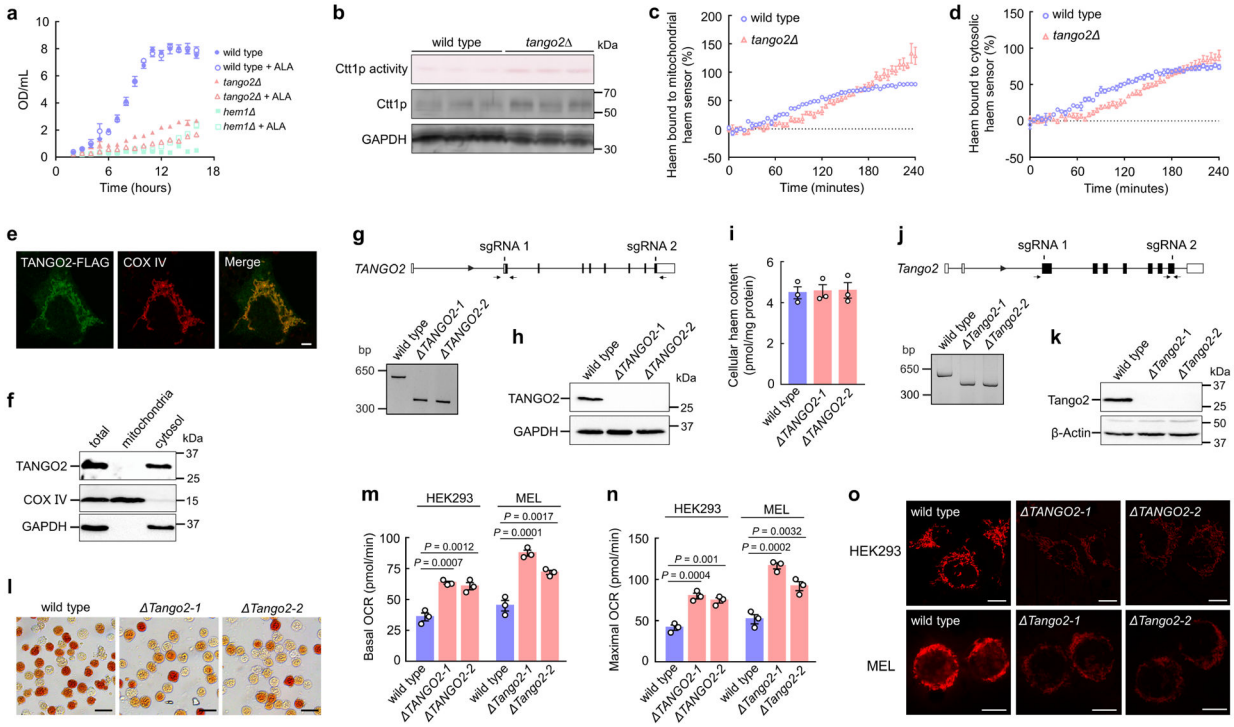

Extended Data Fig. 3 |. TANGO2 proteins regulate haem homeostasis in yeast and mammalian cells.

a, Growth curve of wild type, *hem1Δ*, and *tango2Δ* yeast cells treated with or without 5-aminolevulinic acid (ALA). OD, optical density at 600 nm. n = 2 technical replicates. **b**, The *tango2Δ* yeast cells exhibit increased expression (middle) and activity (top) of Ctt1p. GAPDH is used as a control. **c**,**d**, Dynamics of haem trafficking to mitochondria (**c**) and the cytosol (**d**) in wild type and *tango2Δ* cells. Labile haem levels in mitochondria and the cytosol were monitored by measuring fractional saturation of the haem sensors specifically targeted to these two locations, respectively, following initiation of haem synthesis. **e**, Flag-tagged human TANGO2 colocalizes with the mitochondrial marker COX IV in HEK293 cells. Scale bars, 10 μm. **f**, Western analysis of TANGO2 in whole lysates as well as the mitochondrial and non-mitochondrial fractions of HEK293 cells. The mitochondrial protein COX IV and the cytosolic protein GAPDH were used as controls. **g**, Strategy to knock out *TANGO2* in HEK293 cells and verification of the knockout by genotyping. The sgRNA targeting sites and the positions of genotyping primers are indicated. **h**, Immunoblotting analysis validating the knockout of *TANGO2* in HEK293 cells. **i**, Total haem content of the wild type and *ΔTANGO2* HEK293 cells after treatment with succinylacetone (SA) for 24 h. **j**, Strategy to knock out *Tango2* in MEL cells and verification by PCR genotyping. The sgRNA targeting sites and the positions of genotyping primers are indicated. **k**, Immunoblotting analysis validating the knockout of *Tango2* in MEL cells. **l**, *o*-dianisidine staining of haemoglobin in wild type and *Tango2*-knockout MEL cells. Scale bar, 20 μm. **m**,**n**, Basal oxygen consumption rates (OCR, **m**) and maximal OCR (**n**) of wild type and *TANGO2*-knockout HEK293 and MEL cells. **o**, Representative images of TMRE staining in wild type and *TANGO2*-knockout HEK293 and MEL cells. Scale bars, 20 μm. n = 3

independent experiments for **c**,**d**,**i**,**m**,**n**. Data in **a**,**c**,**d**,**i**,**m**,**n** are presented as mean ± s.e.m. *P* values were determined by one-way ANOVA followed by Tukey's test.

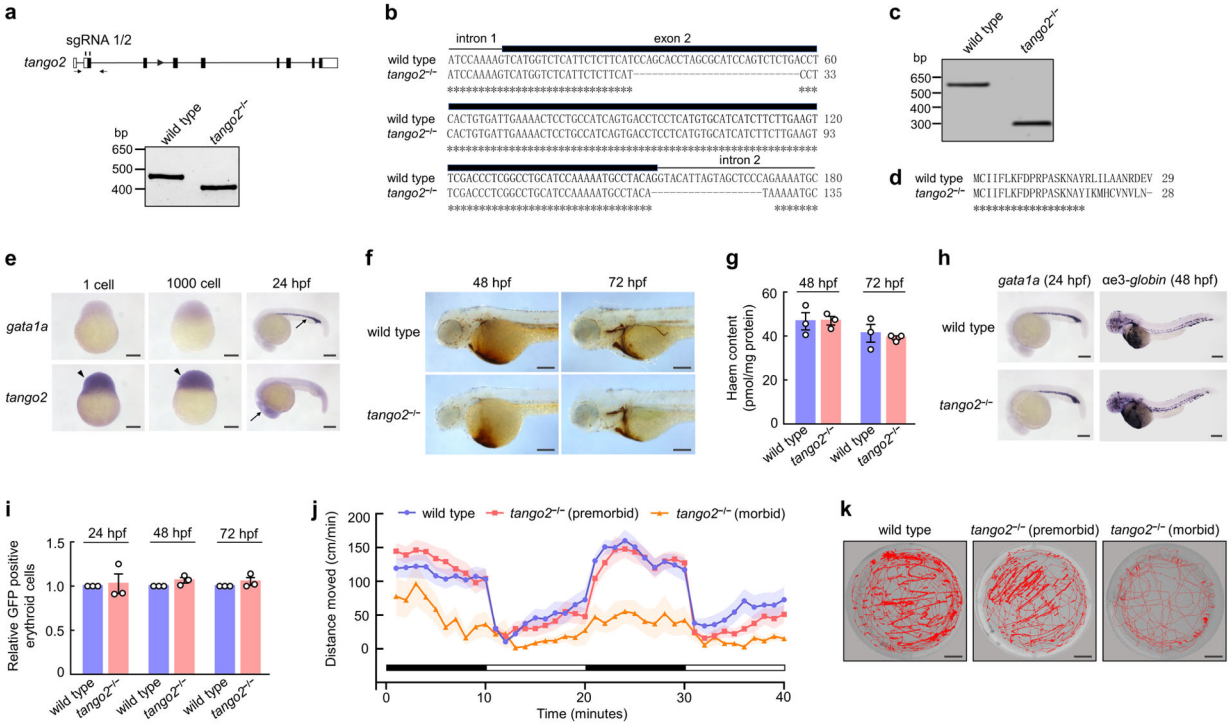

Extended Data Fig. 4 |. Loss of *tango2* leads to reduced locomotor activity of zebrafish larvae. **a**, Strategy to knock out *tango2* in zebrafish and verification of the knockout by PCR genotyping. The sgRNA targeting sites and the positions of PCR primers are indicated. **b**, Comparison of the sequences between the wild type *tango2* and the mutated allele in zebrafish. The exon2 - intron2 junction is deleted in the mutant allele. **c**, Verification of intron 2 retention in the *tango2*$^{-/-}$ zebrafish at the mRNA level by reverse transcription (RT)-PCR. **d**, The predicted protein product of Tango2 in *tango2*$^{-/-}$ zebrafish. **e**, Whole-mount in situ hybridization showing maternal expression of zebrafish *tango2*. Arrowheads indicate the expression of *tango2* in 1-cell and 1000-cell stage embryos. Arrows indicate the expression of *gata1* (control) in the intermediate cell mass and *tango2* in neuronal tissues at 24 h post-fertilization (hpf). Scale bars, 200 μm. **f**, *o*-dianisidine staining of wild type and *tango2*-knockout zebrafish embryos at 48 and 72 hpf. Scale bars, 200 μm. **g**, Total haem content in wild type and *tango2*-knockout zebrafish embryos at 48 and 72 hpf. n = 3 independent experiments. Data are presented as mean ± s.e.m. **h**, Whole-mount in situ hybridization showing normal expression of the erythroid markers *gata1* and *αe3-globin* in *tango2*-knockout zebrafish embryos. Scale bars, 200 μm. **i**, Knockout of *tango2* did not reduce erythrocytes in *Tg(globin-LCR:EGFP)* transgenic zebrafish embryos. n = 3 independent experiments. Data are presented as mean ± s.e.m. **j**, Distance travelled per minute by 12-dpf wild type and *tango2*-knockout zebrafish larvae during the 10-min dark / 10-min light cycles. Black bars indicate dark and white bars indicate light. n = 16 fish for each group. **k**, Representative swimming tracks of 12-dpf wild type and *tango2*-knockout

zebrafish larvae over a 40-min period under constant light. Scale bars, 2.5 mm. Statistical significance was determined by one-way ANOVA followed by Tukey's test.

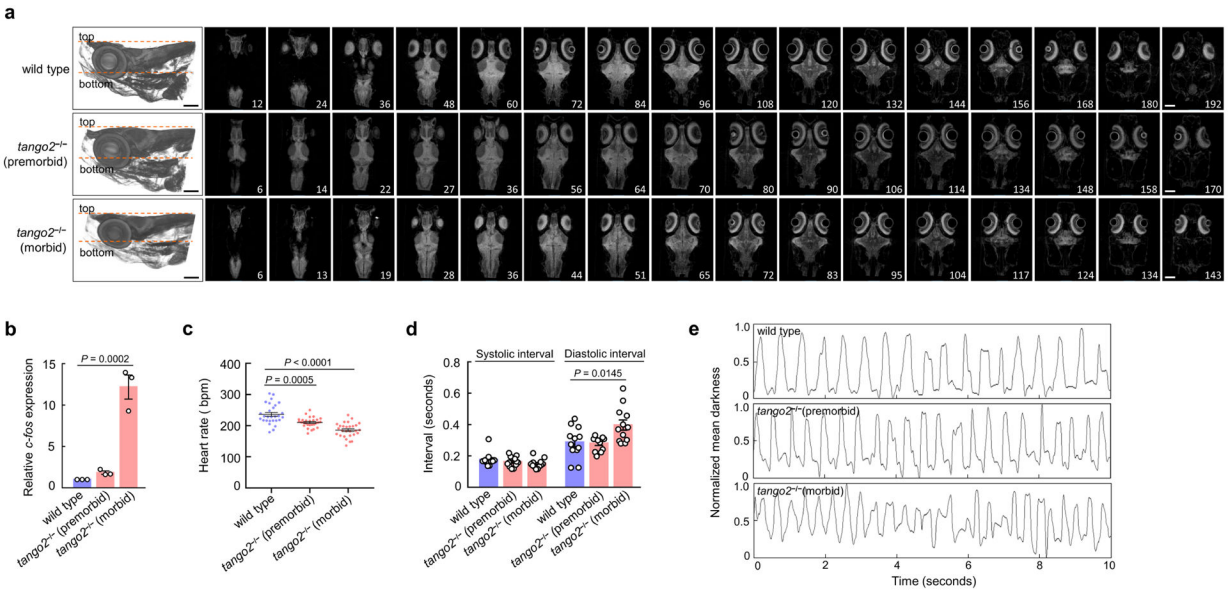

Extended Data Fig. 5 |. Knockout of *tango2* causes brain and heart defects in zebrafish larvae. **a**, Representative micro-CT images of the brains of wild type and *tango2*-knockout zebrafish larvae at 12 dpf. Images on the left are side views of the 3D reconstructed zebrafish brains. Numbers in the images indicate the distance (μm) from the top of the brain, as shown in the 3D images. Scale bars, 100 μm. **b**, Quantitative RT-PCR analysis of *c-fos* in wild type and *tango2*-knockout zebrafish larvae at 12 dpf. Data are presented as mean ± s.e.m from 3 independent experiments. Each sample contains a pool of 30 zebrafish larvae. **c**, Heart rates of wild type and *tango2*-knockout zebrafish larvae at 12 dpf. n = 28 fish for each group. Data are presented as mean ± s.e.m. **d**, Measurement of systolic time interval and diastolic time interval in wild type and *tango2*-knockout zebrafish larvae at 7 dpf. n = 12 fish for each group. Data are presented as mean ± s.e.m. **e**, Detection of heart contractions in 7-dpf wild type and *tango2*-knockout zebrafish larvae using the Changing Pixel Intensity Algorithm. Peaks indicate individual heart contractions. *P* values were determined by one-way ANOVA followed by Tukey's test.

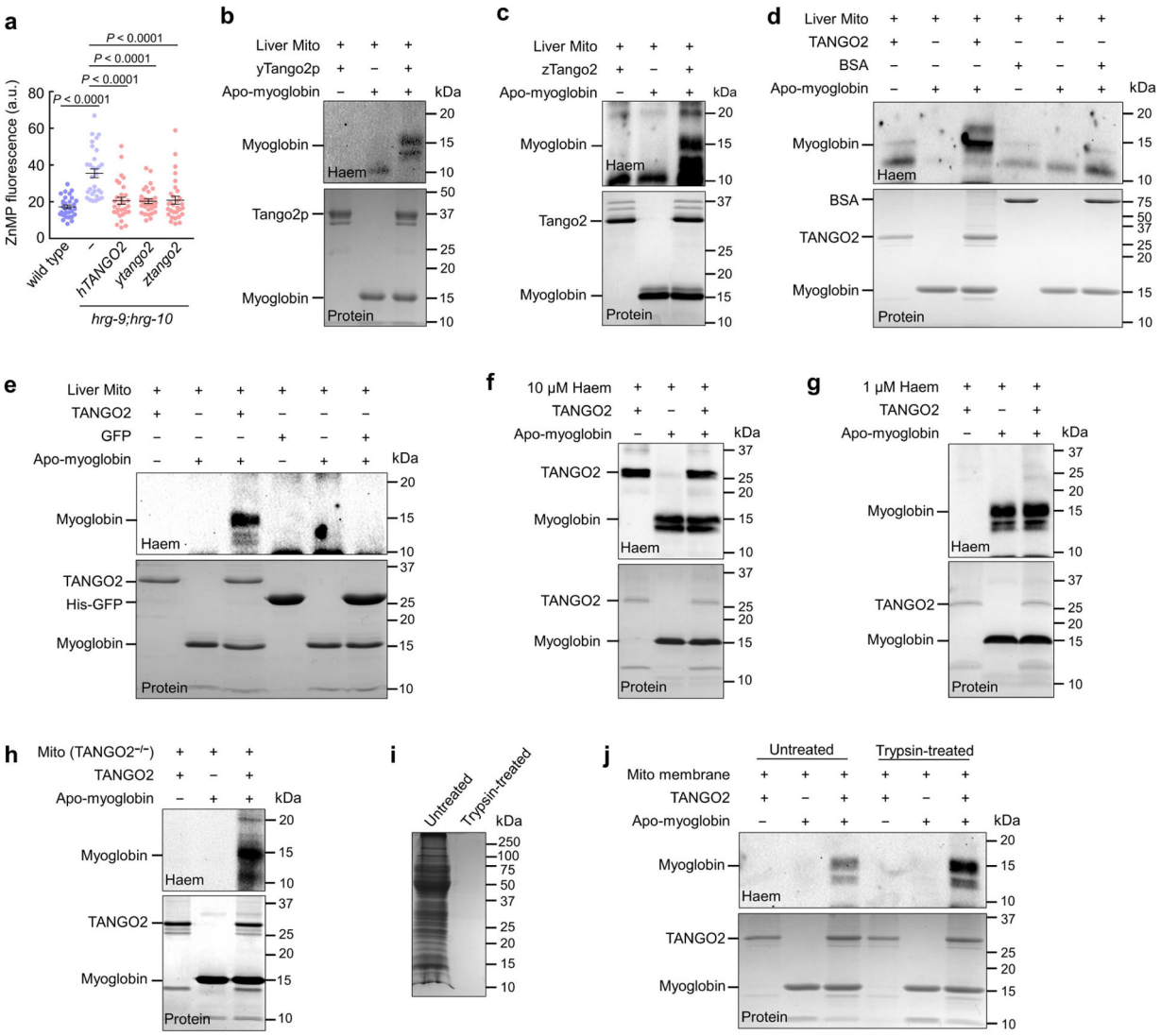

Extended Data Fig. 6 |. TANGO2 transfers haem in vitro.

a, Quantification of ZnMP fluorescence in wild type, *hrg-9* and *hrg-10* double knockout worms, and the double knockout worms expressing *TANGO2* genes from human (*hTANGO2*), yeast (*ytango2*), or zebrafish (*ztango2*). n = 30 worms examined over 3 independent experiments. Data are presented as mean ± s.e.m. *P* values were determined by one-way ANOVA followed by Tukey's test. **b**,**c**, Haem transfer from mitochondria isolated from mouse liver to apo-myoglobin in the absence or presence of yeast Tango2p (**b**) and zebrafish Tango2 (**c**). **d**,**e**, Haem transfer assays for human TANGO2, BSA (**d**), and GFP (**e**). Mitochondria isolated from mouse liver were used as the haem donor and apo-myoglobin was used as the haem acceptor. **f**,**g**, Incorporation of 10 μM (**f**) and 1 μM (**g**) haem into apo-myoglobin in the absence or presence of TANGO2. **h**, Haem transfer from the mitochondria isolated from *TANGO2*-knockout HEK293 cells to apo-myoglobin in the absence or presence of TANGO2. **i**, Coomassie blue staining validating the protein digestion by trypsin in mitochondrial membranes isolated from mouse liver. **j**, Haem transfer

from protein-free mitochondrial membranes to apo-myoglobin in the absence or presence of TANGO2. Mito, mitochondria.

Supplementary Material

Refer to Web version on PubMed Central for supplementary material.

Acknowledgements

We thank R. Lill and H. Gao for critical discussions; the Caenorhabditis Genetics Center (CGC), the B. Grant laboratory, and the A. Soukas laboratory for the worm strains used in this study. This work was supported by funding from the National Natural Science Foundation of China (31871200, 31930003 and 32071155 to C.C.), the National Key Research and Development Program of China (2018YFA0507802 to C.C.), the US National Science Foundation (1552791 to A.R.R.), and the US National Institutes of Health (R33ES025661 to A.R.R. and I.H., R35GM145350 to A.R.R., and R01DK074797 to I.H.).

Data availability

RNA-seq data have been deposited in the Gene Expression Omnibus (GEO) under accession number GSE198848. Gene information for *C. elegans hrg-9* (*R186.1*) and *hrg-10* (*Y80D3A.9*) are available from Wormbase (https://wormbase.org). Source data are provided with this paper.

References

1. Severance S & Hamza I Trafficking of heme and porphyrins in metazoa. Chem. Rev 109, 4596–4616 (2009). [PubMed: 19764719]
2. Reddi AR & Hamza I Heme mobilization in animals: a metallolipid's journey. Acc. Chem. Res 49, 1104–1110 (2016). [PubMed: 27254265]
3. Chambers IG, Willoughby MM, Hamza I & Reddi AR One ring to bring them all and in the darkness bind them: the trafficking of heme without deliverers. Biochim. Biophys. Acta 1868, 118881 (2021).
4. Kremer LS et al. Bi-allelic truncating mutations in *TANGO2* cause infancy-onset recurrent metabolic crises with encephalocardiomyopathy. Am. J. Hum. Genet 98, 358–362 (2016). [PubMed: 26805782]
5. Lalani SR et al. Recurrent muscle weakness with rhabdomyolysis, metabolic crises, and cardiac arrhythmia due to bi-allelic TANGO2 mutations. Am. J. Hum. Genet 98, 347–357 (2016). [PubMed: 26805781]
6. Mingirulli N et al. Clinical presentation and proteomic signature of patients with TANGO2 mutations. J. Inherit. Metab. Dis 43, 297–308 (2020). [PubMed: 31339582]
7. Milev MP et al. The phenotype associated with variants in TANGO2 may be explained by a dual role of the protein in ER-to-Golgi transport and at the mitochondria. J. Inherit. Metab. Dis 44, 426–437 (2021). [PubMed: 32909282]
8. Powell AR, Ames EG, Knierbein EN, Hannibal MC & Mackenzie SJ Symptom prevalence and genotype–phenotype correlations in patients with *TANGO2*-related metabolic encephalopathy and arrhythmias (TRMEA). Pediatr. Neurol 119, 34–39 (2021). [PubMed: 33845444]
9. Rao AU, Carta LK, Lesuisse E & Hamza I Lack of heme synthesis in a free-living eukaryote. Proc. Natl Acad. Sci. USA 102, 4270–4275 (2005). [PubMed: 15767563]
10. Rajagopal A et al. Haem homeostasis is regulated by the conserved and concerted functions of HRG-1 proteins. Nature 453, 1127–1131 (2008). [PubMed: 18418376]
11. Chen C, Samuel TK, Sinclair J, Dailey HA & Hamza I An intercellular heme-trafficking protein delivers maternal heme to the embryo during development in *C. elegans*. Cell 145, 720–731 (2011). [PubMed: 21620137]

12. Korolnek T, Zhang J, Beardsley S, Scheffer GL & Hamza I Control of metazoan heme homeostasis by a conserved multidrug resistance protein. Cell Metab. 19, 1008–1019 (2014). [PubMed: 24836561]
13. Sinclair J et al. Inter-organ signalling by HRG-7 promotes systemic haem homeostasis. Nat. Cell Biol 19, 799–807 (2017). [PubMed: 28581477]
14. Bard F et al. Functional genomics reveals genes involved in protein secretion and Golgi organization. Nature 439, 604–607 (2006). [PubMed: 16452979]
15. Grant B & Hirsh D Receptor-mediated endocytosis in the *Caenorhabditis elegans* oocyte. Mol. Biol. Cell 10, 4311–4326 (1999). [PubMed: 10588660]
16. Schroeder LK et al. Function of the *Caenorhabditis elegans* ABC transporter PGP-2 in the biogenesis of a lysosome-related fat storage organelle. Mol. Biol. Cell 18, 995–1008 (2007). [PubMed: 17202409]
17. O'Rourke EJ, Soukas AA, Carr CE & Ruvkun GC *elegans* major fats are stored in vesicles distinct from lysosome-related organelles. Cell Metab. 10, 430–435 (2009). [PubMed: 19883620]
18. Chen AJ et al. Label-free imaging of heme dynamics in living organisms by transient absorption microscopy. Anal. Chem 90, 3395–3401 (2018). [PubMed: 29401392]
19. Hanna DA et al. Heme dynamics and trafficking factors revealed by genetically encoded fluorescent heme sensors. Proc. Natl Acad. Sci. USA 113, 7539–7544 (2016). [PubMed: 27247412]
20. Ebert PS, Hess RA, Frykholm BC & Tschudy DP Succinylacetone, a potent inhibitor of heme biosynthesis: effect on cell growth, heme content and delta-aminolevulinic acid dehydratase activity of malignant murine erythroleukemia cells. Biochem. Biophys. Res. Commun 88, 1382–1390 (1979). [PubMed: 289386]
21. Williams CC, Jan CH & Weissman JS Targeting and plasticity of mitochondrial proteins revealed by proximity-specific ribosome profiling. Science 346, 748–751 (2014). [PubMed: 25378625]
22. Martinez-Guzman O et al. Mitochondrial–nuclear heme trafficking in budding yeast is regulated by GTPases that control mitochondrial dynamics and ER contact sites. J. Cell Sci 133, jcs237917 (2020). [PubMed: 32265272]
23. Yuan X et al. Regulation of intracellular heme trafficking revealed by subcellular reporters. Proc. Natl Acad. Sci. USA 113, E5144–E5152 (2016). [PubMed: 27528661]
24. Li Y et al. MFSD7C switches mitochondrial ATP synthesis to thermogenesis in response to heme. Nat. Commun 11, 4837 (2020). [PubMed: 32973183]
25. Chiabrando D et al. The mitochondrial heme exporter FLVCR1b mediates erythroid differentiation. J. Clin. Invest 122, 4569–4579 (2012). [PubMed: 23187127]
26. Galmozzi A et al. PGRMC2 is an intracellular haem chaperone critical for adipocyte function. Nature 576, 138–142 (2019). [PubMed: 31748741]
27. Lev S Non-vesicular lipid transport by lipid-transfer proteins and beyond. Nat. Rev. Mol. Cell Biol 11, 739–750 (2010). [PubMed: 20823909]
28. Holthuis JC & Menon AK Lipid landscapes and pipelines in membrane homeostasis. Nature 510, 48–57 (2014). [PubMed: 24899304]
29. Giri RP et al. Continuous uptake or saturation-investigation of concentration and surface-packing-specific hemin interaction with lipid membranes. J. Phys. Chem. B 122, 7547–7554 (2018). [PubMed: 29983065]
30. Garber Morales J et al. Biophysical characterization of iron in mitochondria isolated from respiring and fermenting yeast. Biochemistry 49, 5436–5444 (2010). [PubMed: 20536189]
31. Ganis JJ et al. Zebrafish globin switching occurs in two developmental stages and is controlled by the LCR. Dev. Biol 366, 185–194 (2012). [PubMed: 22537494]
32. Gietz RD & Schiestl RH Applications of high efficiency lithium acetate transformation of intact yeast cells using single-stranded nucleic acids as carrier. Yeast 7, 253–263 (1991). [PubMed: 1882550]
33. Ness F et al. Sterol uptake in *Saccharomyces cerevisiae* heme auxotrophic mutants is affected by ergosterol and oleate but not by palmitoleate or by sterol esterification. J. Bacteriol 180, 1913–1919 (1998). [PubMed: 9537392]

34. Sinclair PR, Gorman N & Jacobs JM Measurement of heme concentration. Curr. Protoc. Toxicol 8, Unit 8.3 (2001).
35. Chen C et al. Snx3 regulates recycling of the transferrin receptor and iron assimilation. Cell Metab. 17, 343–352 (2013). [PubMed: 23416069]
36. Dickinson DJ, Ward JD, Reiner DJ & Goldstein B Engineering the Caenorhabditis elegans genome using Cas9-triggered homologous recombination. Nat. Methods 10, 1028–1034 (2013). [PubMed: 23995389]
37. Kang J et al. *Caenorhabditis elegans* homologue of Fam210 is required for oogenesis and reproduction. J. Genet. Genomics 47, 694–704 (2020). [PubMed: 33547005]
38. Arribere JA et al. Efficient marker-free recovery of custom genetic modifications with CRISPR/Cas9 in *Caenorhabditis elegans*. Genetics 198, 837–846 (2014). [PubMed: 25161212]
39. Picelli S et al. Full-length RNA-seq from single cells using Smart-seq2. Nat. Protoc 9, 171–181 (2014). [PubMed: 24385147]
40. McGhee JD et al. ELT-2 is the predominant transcription factor controlling differentiation and function of the *C. elegans* intestine, from embryo to adult. Dev. Biol 327, 551–565 (2009). [PubMed: 19111532]
41. Kim D, Langmead B & Salzberg SL HISAT: a fast spliced aligner with low memory requirements. Nat. Methods 12, 357–360 (2015). [PubMed: 25751142]
42. Pertea M et al. StringTie enables improved reconstruction of a transcriptome from RNA-seq reads. Nat. Biotechnol 33, 290–295 (2015). [PubMed: 25690850]
43. Robinson MD, McCarthy DJ & Smyth GK edgeR: a Bioconductor package for differential expression analysis of digital gene expression data. Bioinformatics 26, 139–140 (2010). [PubMed: 19910308]
44. Zhen R et al. Wdr26 regulates nuclear condensation in developing erythroblasts. Blood 135, 208–219 (2020). [PubMed: 31945154]
45. Thisse C & Thisse B High-resolution in situ hybridization to whole-mount zebrafish embryos. Nat. Protoc 3, 59–69 (2008). [PubMed: 18193022]
46. Fink M et al. A new method for detection and quantification of heartbeat parameters in Drosophila, zebrafish, and embryonic mouse hearts. Biotechniques 46, 101–113 (2009). [PubMed: 19317655]
47. Kawahara G, Guyon JR, Nakamura Y & Kunkel LM Zebrafish models for human FKRP muscular dystrophies. Hum. Mol. Genet 19, 623–633 (2010). [PubMed: 19955119]
48. Unissa AN, Subbian S, Hanna LE & Selvakumar N Overview on mechanisms of isoniazid action and resistance in Mycobacterium tuberculosis. Infect. Genet. Evol 45, 474–492 (2016). [PubMed: 27612406]
49. Unissa AN et al. Significance of catalase-peroxidase (KatG) mutations in mediating isoniazid resistance in clinical strains of *Mycobacterium tuberculosis*. J. Glob. Antimicrob. Resist 15, 111–120 (2018). [PubMed: 29990547]
50. Hanna DA et al. Heme bioavailability and signaling in response to stress in yeast cells. J. Biol. Chem 293, 12378–12393 (2018). [PubMed: 29921585]
51. Baureder M, Reimann R & Hederstedt L Contribution of catalase to hydrogen peroxide resistance in Enterococcus faecalis. FEMS Microbiol. Lett 331, 160–164 (2012). [PubMed: 22486165]
52. Ran FA et al. Genome engineering using the CRISPR–Cas9 system. Nat. Protoc 8, 2281–2308 (2013). [PubMed: 24157548]
53. Chen W et al. Abcb10 physically interacts with mitoferrin-1 (Slc25a37) to enhance its stability and function in the erythroid mitochondria. Proc. Natl Acad. Sci. USA 106, 16263–16268 (2009). [PubMed: 19805291]
54. Feissner R, Xiang Y & Kranz RG Chemiluminescent-based methods to detect subpicomole levels of c-type cytochromes. Anal. Biochem 315, 90–94 (2003). [PubMed: 12672416]
55. Piel RB 3rd et al. A novel role for progesterone receptor membrane component 1 (PGRMC1): a partner and regulator of ferrochelatase. Biochemistry 55, 5204–5217 (2016). [PubMed: 27599036]

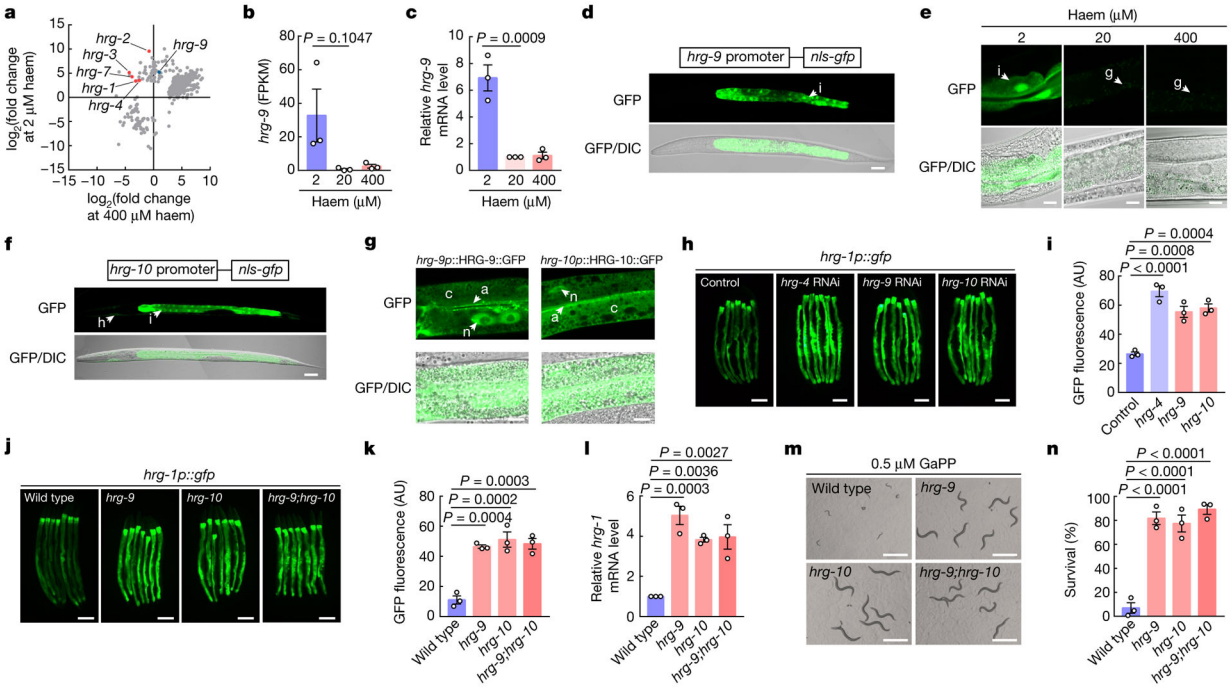

Fig. 1 |. *hrg-9* regulates haem homeostasis in *C. elegans*.

a, Genes with altered expression at low (2 µM) or high (400 µM) haem (versus 20 µM haem) from transcriptomics analysis of *C. elegans* intestine. Previously reported haem-responsive genes are highlighted in red and *R186.1* (also known as *hrg-9*) is shown in blue. **b**, *hrg-9* quantification from the RNA-seq experiment on intestines isolated from worms growing at different haem concentrations. $n = 3$ for each group. FPKM, fragments per kilobase of transcript per million mapped reads. **c**, RT–qPCR analyses of *hrg-9* expression in worms growing at different haem concentrations. **d**, Schematic (top) and expression (middle and bottom) of the *hrg-9p::nls-gfp* transgene in *C. elegans*. Scale bar, 20 µm. DIC, differential interference contrast microscopy; i, intestine. **e**, Haem regulates the expression of *hrg-9p::nls-gfp* reporter. Scale bars, 20 µm. g, gut granules. **f**, Schematic (top) and expression (middle and bottom) of *hrg-10p::nls-gfp* reporter in *C. elegans*. Scale bar, 20 µm. h, hypodermis. **g**, Subcellular localization of HRG-9::GFP and HRG-10::GFP in *C. elegans* intestinal cells. Scale bars, 10 µm. c, cytoplasm; n, nucleus; a, apical plasma membrane. **h**,**i**, Representative images (**h**) and quantification (**i**) of *hrg-1p::gfp* expression in worms with indicated RNAi. Scale bars, 100 µm. AU, arbitrary units. **j**,**k**, Representative images (**j**) and quantification (**k**) of *hrg-1p::gfp* expression in wild-type and *hrg-9*-, *hrg-10*- and *hrg-9;hrg-10*-knockout worms. Scale bars, 100 µm. **l**, Quantification of endogenous *hrg-1* mRNA by RT–qPCR in worms with indicated genotypes. **m**, Representative images of worms of the indicated genotypes after exposure to 0.5 µM GaPP for 3 days. Scale bars, 1 mm. **n**, Survival of worms of the indicated genotypes after exposure to 1 µM GaPP for 4 days. $n = 3$ independent experiments in **c**,**i**,**k**,**l**,**n**. Data in **b**,**c**,**i**,**k**,**l**,**n** are mean ± s.e.m. One-way ANOVA followed by Tukey's test.

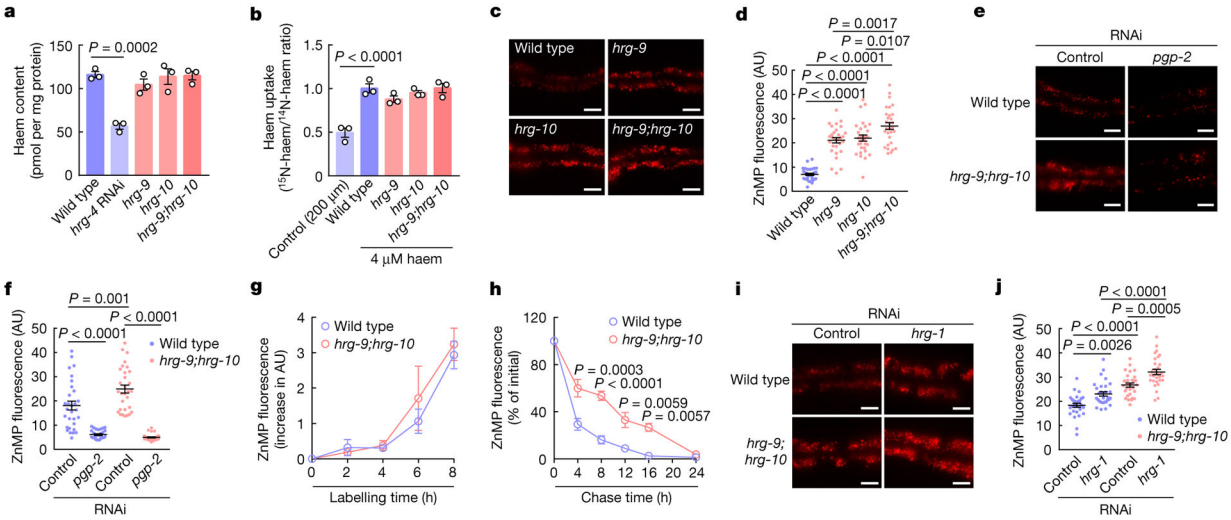

Fig. 2 |. Loss of *hrg-9* and *hrg-10* results in haem accumulation in LROs.

a, Total haem content in the worms of indicated genotypes. *hrg-4* RNAi was used as a control. $n = 3$ independent experiments. **b**, Haem uptake in the worms of indicated genotypes. Wild-type worms cultured with 200 μM haem were used as a control. $n = 3$ independent experiments. **c**,**d**, Representative images (**c**) and quantification (**d**) of ZnMP staining in the worms of indicated genotypes. $n = 30$ worms examined over 3 independent experiments. Scale bars, 20 μm. **e**,**f**, Representative images (**e**) and quantification (**f**) of ZnMP fluorescence in wild-type and *hrg-9* and *hrg-10* double-knockout worms treated with control or *pgp-2* RNAi. $n = 30$ worms examined over 3 independent experiments. Scale bars, 20 μm. **g**,**h**, Quantification of ZnMP fluorescence during ZnMP pulse (**g**) and chase (**h**) analyses in wild-type and *hrg-9* and *hrg-10* double-knockout worms. $n = 36$ worms examined over 3 independent experiments. **i**,**j**, Representative images (**i**) and quantification (**j**) of ZnMP fluorescence in wild-type and *hrg-9* and *hrg-10* double-knockout worms treated with control or *hrg-1* RNAi. $n = 30$ worms examined over 3 independent experiments. Scale bars, 20 μm. Data in **a**,**b**,**d**,**f**–**h**,**j** are mean ± s.e.m. One-way ANOVA followed by Tukey's test.

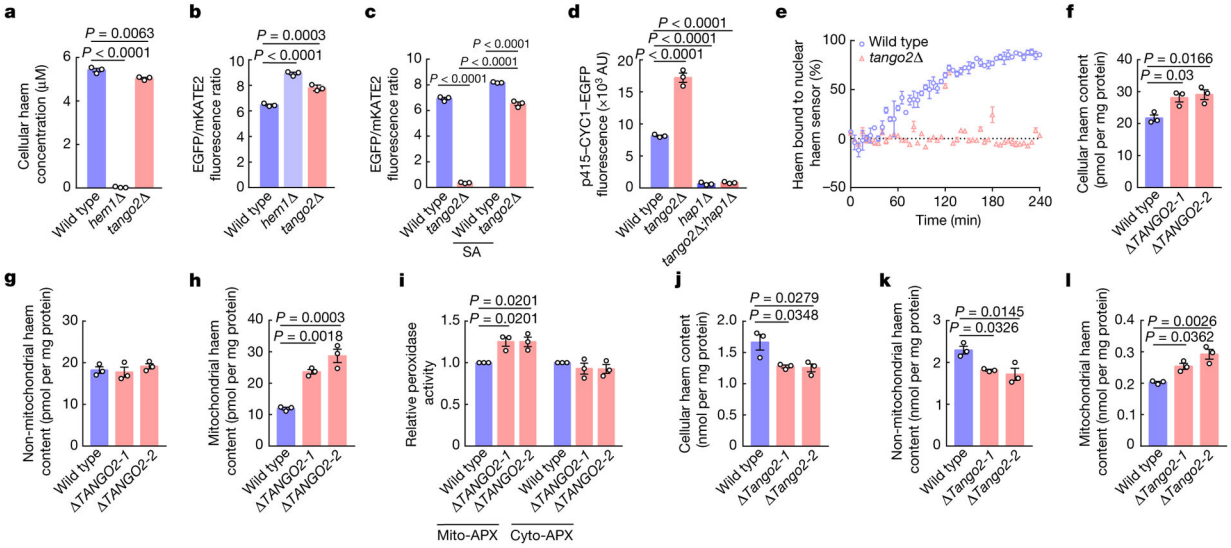

Fig. 3 |. TANGO2 regulates mitochondrial haem homeostasis in yeast and mammalian cells.
a, Total haem content in wild-type, *hem1Δ* and *tango2Δ* yeast cells. **b**, The ratio of EGFP to mKATE2 fluorescence for cytosolic haem sensor expressed in wild-type, *hem1Δ*, and *tango2Δ* yeast cells. The ratio correlates inversely with labile haem in the cytosol. **c**, The EGFP/mKATE2 fluorescence ratio for mitochondrial haem sensor in wild-type and *tango2Δ* yeast cells treated with or without 0.5 mM succinylacetone (SA). The ratio correlates inversely with the labile haem in mitochondria. **d**, Hap1 reporter activity as assessed by fluorescence of the indicated p415–CYC1–EGFP-expressing yeast cells. **e**, Dynamics of haem trafficking to the nuclei of wild-type and *tango2Δ* yeast cells. Labile haem in nuclei was monitored by measuring the fractional saturation of the nuclear haem sensor following initiation of haem synthesis. **f**–**h**, Haem content in total lysates (**f**), non-mitochondrial fractions (**g**) and mitochondrial fractions (**h**) of wild-type and *TANGO2*-knockout HEK293 cells. **i**, Activity of ascorbate peroxidase expressed in the mitochondria (mito-APX) or cytoplasm (cyto-APX) of wild-type and *ΔTANGO2* HEK293 cells. **j**–**l**, Haem content in total lysates (**j**), non-mitochondrial fractions (**k**) and mitochondrial fractions (**l**) of wild-type and *Tango2*-knockout MEL cells. All experiments were performed three times. Data are mean ± s.e.m. One-way ANOVA followed by Tukey's test.

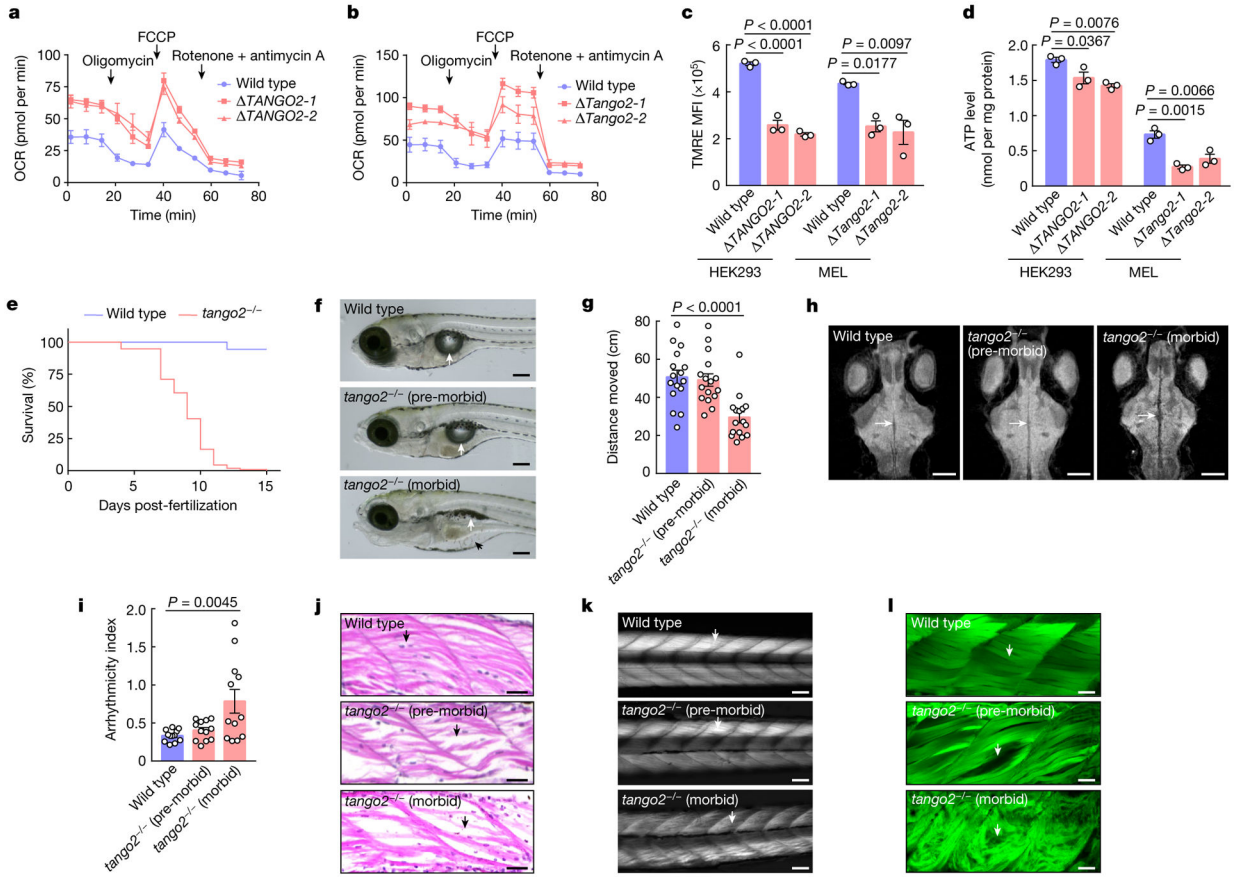

Fig. 4 |. *TANGO2* deficiency leads to mitochondrial defects in mammalian cells and lethality in zebrafish.

a,**b**, Oxygen consumption rate (OCR) of wild-type and *TANGO2*-knockout HEK293 (**a**) and MEL (**b**) cells. **c**, Flow cytometric analysis of tetramethylrhodamine ethyl ester (TMRE) staining in wild-type and *TANGO2*-knockout HEK293 and MEL cells. MFI, mean fluorescence intensity. **d**, ATP concentration in wild-type and *TANGO2*-knockout HEK293 and MEL cells. **e**, Survival curve of wild-type (n = 124) and *tango2*-knockout (n = 114) zebrafish. **f**, Representative images of wild-type and *tango2*-knockout zebrafish larvae at 12 days post-fertilization (dpf). The *tango2*$^{-/-}$ larvae are shown under both pre-morbid and morbid conditions. Black arrow indicates pericardial oedema and white arrows indicate the swim bladder. Scale bars, 0.2 mm. **g**, The distance travelled by 12-dpf wild-type and *tango2*-knockout zebrafish larvae over a 40-min period. n = 16 fish for each group. **h**, Representative micro-CT images of brains from wild-type and *tango2*-knockout zebrafish larvae at 12 dpf. Arrows indicate longitudinal fissures. Scale bars, 100 μm. **i**, The arrhythmicity index of wild-type and *tango2*-knockout zebrafish larvae at 7 dpf. n = 12 fish for each group. **j**, Haematoxylin and eosin-stained muscle sections from wild-type and *tango2*-knockout zebrafish larvae at 12 dpf. Arrows indicate muscle fibres. Scale bars, 20 μm. **k**,**l**, Images of birefringence (**k**) and phalloidin staining (**l**) of wild-type and *tango2*-knockout zebrafish larvae at 12 dpf. Arrows indicate muscle fibres. Scale bars are 50 μm (**k**) and 20 μm (**l**). **a**–**d**, n = 3 independent experiments. Data in **a**–**d**,**g**,**i** are mean ± s.e.m. One-way ANOVA followed by Tukey's test.

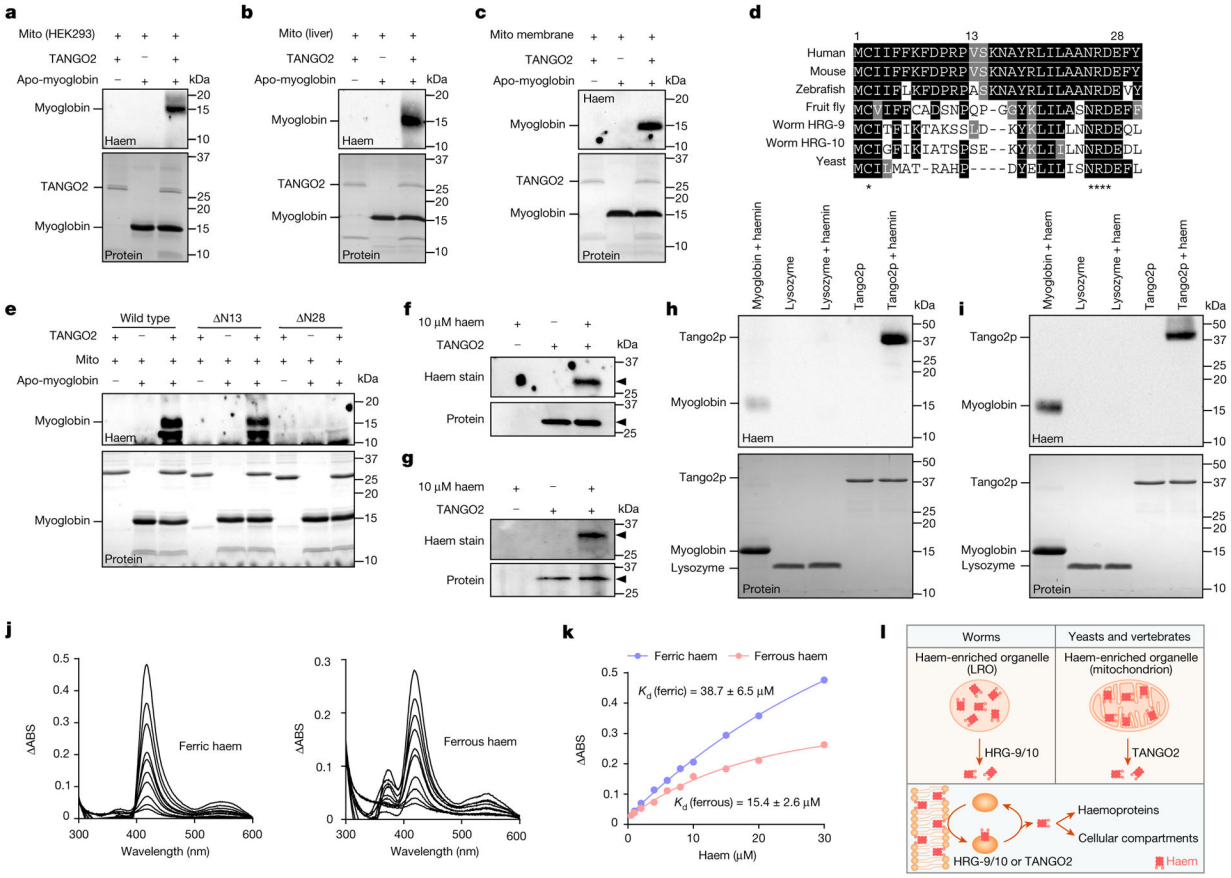

Fig. 5 |. TANGO2 binds to and transfers haem in vitro.

a,**b**, Haem transfer from mitochondria (mito) isolated from HEK293 cells (**a**) or mouse liver (**b**) to apo-myoglobin in the absence or presence of TANGO2. **c**, Haem transfer from mitochondrial membranes isolated from mouse liver to apo-myoglobin in the absence or presence of TANGO2. **d**, Sequence alignment of the N-terminal regions of HRG-9 and TANGO2 proteins. **e**, Haem transfer assays for the full-length TANGO2 and TANGO2 lacking the N-terminal 13 (ΔN13) or 28 (ΔN28) amino acids. Mitochondria isolated from mouse liver were used as the haem donor and apo-myoglobin was used as the haem acceptor. **f**,**g**, Haem activity assay (top) and immunoblotting analysis (bottom) of human (**f**) and mouse (**g**) TANGO2–Flag before and after incubation with haem in the presence of sodium dithionite. Human and mouse TANGO2–Flag were expressed and purified from HEK293 cells and MEL cells, respectively. Arrowheads indicate human or mouse TANGO2–Flag. **h**,**i**, Haem activity assay (top) and Coomassie staining (bottom) of yeast Tango2p before and after incubation with haem in the absence (**h**) or presence (**i**) of sodium dithionite. Myoglobin and lysozyme were used as positive and negative controls, respectively. **j**, Subtractive absorption spectra (ΔABS) of yeast Tango2p with increasing concentrations of haem in the absence (ferric haem) or presence (ferrous haem) of sodium dithionite. Differential absorbance was monitored at 419 nm and 414 nm for binding assays with ferric and ferrous haem, respectively. **k**, Data from **j** was used to calculate the dissociation constant (K_d). **l**, Proposed model of the role of HRG-9 or HRG-10 (HRG-9/10) and TANGO2 in regulating intracellular haem homeostasis. In haem

auxotrophs (worms) and haem-synthesizing eukaryotes (yeasts and vertebrates), HRG-9/10 and TANGO2 translocate haem out of the haem storage site (LRO) and haem synthesis site (mitochondrion), respectively. HRG-9/10 and TANGO2 may transfer haem from haem-enriched membranes. Mito, mitochondria.